



DISSERTATION ACCEPTANCE CERTIFICATE

The undersigned, appointed by the
Division of Medical Sciences

Program in Neuroscience

have examined a dissertation entitled

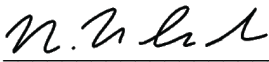
A Neuron in the Visual System That Provides Feedback About Limb Movement

presented by Alexandra Kaye Hartman

candidate for the degree of Doctor of Philosophy and hereby
certify that it is worthy of acceptance.

Signature: 
John A. Assad (Apr 12, 2024 12:00 EDT)

Typed Name: Dr. John Assad

Signature: 

Typed Name: Dr. Naoshige Uchida

Signature: 
Mark Andermann (Apr 12, 2024 17:01 EDT)

Typed Name: Dr. Mark Andermann

Signature: 
Andrew Seeds (Apr 12, 2024 11:56 EDT)

Typed Name: Dr. Andrew Seeds

Date: April 12, 2024

A Neuron in the Visual System That Provides Feedback About Limb Movement

A dissertation presented

by

Alexandra Kaye Hartman

to

The Division of Medical Sciences

in partial fulfillment of the requirements

for the degree of

Doctor of Philosophy

in the subject of

Neuroscience

Harvard University

Cambridge, Massachusetts

April 2024

© 2024 Alexandra Kaye Hartman

All rights reserved.

A Neuron in the Visual System That Provides Feedback About Limb Movement

Abstract

Sensory stimuli can arise from the environment and also, predictably, from an organism's own movements. The ability to distinguish between self-generated and external sensory stimuli is essential for normal behavior, but the neural circuits that anticipate and cancel responses to self-motion are not well understood in most organisms and modalities. This study focuses on a previously uncharacterized group of neurons in the *Drosophila* visual system known as LT52 cells. LT52 cells receive the majority of their input from the optic lobes and provide strong inhibitory input to a specialized circuit in the central brain that mediates the visual pursuit of moving objects. To our surprise, we found that LT52 neurons are strongly activated when flies groomed their heads – even in the absence of an external visual stimulus. By comparing activity in genetically blind and control flies, we determined that this activity is partially driven by a non-visual signal. We found that the non-visual component of the response is specifically related to the movement of the ipsilateral foreleg, suggesting that it arises from internal self-motion signals, specifically proprioceptive feedback and/or copies of ipsilateral motor commands. In terms of visual tuning, we found that LT52 neurons respond best to large, fast-moving stimuli with vertically extended edges and have a strong directional preference for motion in the front-to-back direction. We show that these tuning properties overlap with the visual stimulus generated by the fly's leg as it sweeps back and forth across the eye during head grooming, suggesting that LT52 activity during head grooming is also partly driven by visual reafference. The visual tuning of LT52 complements the tuning of its postsynaptic targets, which are small

object motion detectors that respond to slower, more ethologically-relevant speeds. Taken together, our results suggest that LT52 neurons serve to inhibit the postsynaptic population's response to large, fast-moving stimuli that the downstream circuit might otherwise confuse for the movement of a visual target. The movement of the fly's own leg represents a special kind of visual "distractor" whose appearance can be predicted by a combination of visual reafference and internal self-motion signals input to LT52.

Table of Contents

| | |
|--|-----------|
| Title | i |
| Copyright | ii |
| Abstract | iii |
| Table of Contents | v |
| List of Figures | vii |
| Acknowledgements | viii |
| Attributions | x |
| 1. Introduction | 1 |
| 2. Results | 13 |
| 2.1 Experimental overview | 13 |
| 2.2 Activity during head grooming is driven by visual and non-visual input | 13 |
| 2.3 Visual tuning of LT52 matches leg movements during grooming | 24 |
| 3. Discussion | 32 |
| 4. Methods | 39 |
| 4.1 Acknowledgements | 39 |
| 4.2 Fly husbandry and genotypes | 39 |
| 4.3 Fly preparation and dissection | 40 |
| 4.4 Two-photon calcium imaging | 40 |
| 4.5 Measurement of fly locomotion and head grooming | 41 |
| 4.6 Visual stimulus delivery | 41 |

| | |
|------------------------------|-----------|
| 4.7 Data analysis | 43 |
| 5. Bibliography | 46 |

List of Figures

| | |
|---|----|
| Figure 1. Imaging of LT52 activity during head grooming | 14 |
| Figure 2. LT52 activity is inversely correlated with forward velocity | 15 |
| Figure 3. Activity during head grooming is driven by a combination of visual and non-visual input | 17 |
| Figure 4. The ipsilateral leg is a better predictor of LT52 activity | 21 |
| Figure 5. LT52 responses are reduced but not abolished when the ipsilateral leg is stumped | 23 |
| Figure 6. Leg movements during head grooming | 25 |
| Figure 7. Visual tuning properties of LT52 | 28 |

Acknowledgments

This work would not have been possible without the support of many wonderful people. I am especially grateful for my advisor, Rachel Wilson. Thank you, Rachel, for your dedication, patience, wisdom, tenacity, and wonderful sense of humor. It has been such a privilege to be part of your lab and the extraordinary science that's done here. Thank you to all of my fellow Wilson Lab members, past and present – Asa Barth-Maron, Melanie Basnak, Alexander Bates, Alex Batchelor, Matthew Collie, Fernanda Conti, Jingxuan Fan, Yvette Fisher, Stephen Holtz, Chennan Jin, James Jeanne, Emily Kellogg, Jenny Lu, Michael Marquis, Habiba Noamany, Tatsuo Okubo, Diego Pacheco Pinedo, Janki Patel, Paola Patella, Noah Pettit, Pablo Reimers, Sophia Renauld, Sasha Rayshubskiy, Quinn Vanderbeck, Elena Westeinde, Carl Wienecke, Helen Yang, and Wenyi Zhang. You are an incredibly smart and talented group of people. I will really miss you guys.

Thank you to my undergraduate advisor Mike Wehr, who taught me how to think like a scientist, and to all of my friends and mentors at the University of Oregon – Aldis Weible, Michael Kyweriga, Xiang Gao, Joe Wekselblatt, Abe Katzen, Dan Rowland, Leah DeBlander and Katelyn Dufour. I wouldn't be where I am today without your friendship and support. I would also like to thank my defense committee members John Assad, Mark Andermann, Andrew Seeds, and Nao Uchida, DAC members Bruce Bean and Gary Yellen, and my SAC advisor Rick Born. Thank you to PiN coordinators Karen Harmin and Susan Jackson for all of the valuable support they have provided over the years.

Thank you to the incredible group of housemates and friends who weathered the pandemic years with me, especially Anna Meilman, Felix Baier, Julie Murmann, Mert Yilmaz, Mazmodae Banburski-Fahey and Andrzej Banburski-Fahey. Your creativity and camaraderie

brought – and continues to bring! – great joy to my life outside of the lab. I would like to thank my mother, Mona Hartman, for her unconditional love and encouragement in every endeavor I've undertaken, from the silliest to the most serious. I would like to thank my stepfather, Nelson Maler, for being an incredible source of support and a wonderful addition to our family. Thanks also to my brother, Hayes Hartman, who I am incredibly proud of and can always count on for a weird story and a long laugh. Thank you to my extended family – aunts, uncles, cousins, and grandparents – on the West Coast. I am incredibly lucky to be part of such a family and can't wait to spend more time with you all back in the Northwest. Thank you also to my lifelong friends Tyler Artner and Kelly Casey, and to my boyfriend Ross Pergiel for his daily, long-distance support in the last years of my PhD. Lastly, I would like to dedicate this thesis to my late father, Wes Hartman, who was a uniquely compassionate, hardworking, and upstanding person. He continues to be a source of courage and inspiration for me.

Attributions

Matthew Collie and Emily Kellogg identified the split-Gal4 line used in this study. Emily Kellogg performed antibody labeling and confocal imaging, assisted by Chennan Jin. Matt Collie assisted with the visual stimulus display. I collected and analyzed 2-photon calcium imaging data and behavioral data. I wrote the text with the help of Rachel Wilson.

1. Introduction

Body movements create self-generated or “reafferent” sensory stimuli (Sperry, 1950; von Holst and Mittelstaedt, 1950). Self-generated stimuli can be useful because they can provide feedback about the accuracy of voluntary movements. At the same time, they can also be problematic, because they interfere with external sensory stimuli. To deal with this problem, the nervous system has evolved ways to anticipate self-generated stimuli and then subtract them from external stimuli (Cullen, 2004). For example, in primates, the act of initiating a motor saccade is used to generate a prediction of the resulting self-generated optic flow, which is then subtracted from incoming visual signals (Binda and Morrone, 2018; Wurtz, 2018). Similarly, in crickets, the act of producing a chirp is used to generate a prediction of the resulting sound, which is then subtracted from incoming auditory signals (Poulet and Hedwig, 2006, 2007). And, in mormyrid fish, the act of producing an electric field is used to generate a prediction of the resulting electromagnetic chirp, which is then subtracted from incoming electrosensory signals (Bell, 1981; Requarth, Kaifosh and Sawtell, 2014; Fukutomi and Carlson, 2020). The ability to predict self-generated sensory signals is fundamental to our sense of self (Gallagher, 2000): for example, it makes us unable to tickle our own body (Blakemore, Frith and Wolpert, 1999). Conversely, losing the ability to predict self-generated signals may underpin delusions of agency in some psychiatric and neurological disorders (Frith, 1992; Sirigu *et al.*, 1999).

The concept of canceling self-generated stimuli was first proposed in 1950 by two independent research groups. The first report, from the German researchers von Holst and Mittelstaedt, focused on the optokinetic response in the blowfly *Eristalis*, in which flies turn reflexively in response to changes in visual input to maintain gaze stability – for example, if the visual world moves abruptly to the left, the fly will turn to the left to maintain a stable visual

scene. Interestingly, similar changes in the visual scene are created during voluntary turns, yet flies do not show an optokinetic response following self-initiated movements. von Holst and Mittelstaedt proposed that the reason that this does not occur is because an internal “efference copy” signal acts to subtract out the visual system’s response to self-initiated turns. To test this idea, they inverted the direction of visual flow perceived by the fly by rotating its head by 180° on the longitudinal axis. Following a voluntary turn, they found that flies circle continuously in the same direction. This circling behavior indicated that the optokinetic reflex was not broadly inhibited during voluntary turns, but rather that the brain anticipates a specific kind of visual stimulus during movement that is normally neutralized by an internal motor command. If visual flow is reversed, the reafferent visual signal that results from a voluntary turn is enhanced instead of canceled, causing the fly to turn continuously in an effort to stabilize the scene.

The second foundational paper, authored by Roger Sperry, featured a similar set of experiments in pufferfish, which exhibit an optokinetic reflex similar to that seen in the blowfly. Sperry observed the same kind of circling behavior in the pufferfish after covering one of the fish’s eyes with a blinder and rotating the other by 180° to reverse horizontal visual flow. Sperry took his experiment one step further by ablating a number of different brain regions in an effort to identify where the sensory cancellation process occurred, ultimately identifying the optic tectum as the site of visual-motor cancellation. Sperry independently proposed a very similar mechanism to the one proposed by von Holst and Mittelstaedt to explain his result but instead used the phrase “corollary discharge” to refer to the internal signal that results from a motor command.

The common principle that the two studies arrived at – namely, that organisms are capable of predicting the sensory consequence of their actions – is generally referred to as the

reafference principle. Today, the terms efference copy and corollary discharge are often used interchangeably in neuroscientific literature when referring to motor-related signals that provide the basis for sensory prediction. However, it should be noted that some researchers maintain that the two terms have different meanings (Crapse and Sommer, 2008; Straka, Simmers and Chagnaud, 2018; Fukutomi and Carlson, 2020). Specifically, it has been proposed that corollary discharge be used as a general term to describe any motor-related timing signal that influences sensory-motor processing, either through subtraction, facilitation, or some other form of modulation. Efference copy, meanwhile, is argued to have a more narrow definition within the broader category of corollary discharge signals, which is defined as an invariant copy of a motor command that is used as a subtractive signal for the purpose of canceling predictable sensory input.

Following these initial reports, behavioral and physiological evidence for the reafference principle began to emerge in other organisms and modalities. By the 1970s and 80s, researchers had begun to understand how reafference cancellation works at a cellular level, based mostly on work in invertebrate systems.

One of the first circuits to be delineated was found in the sea slug, *Pleurobranchaea californica*. Sea slugs normally exhibit a withdrawal reflex in response to tactile stimulation of the oral veil, a net-like flap of tissue that is used to scan the ocean floor for prey. However, slugs do not exhibit a withdrawal reflex during active feeding, despite the fact that the rhythmic movements that accompany feeding produce a similar, self-generated tactile stimulus (Davis, Siegler and Mpitoses, 1973). Using a combination of electrical stimulation and extracellular recordings in dissected slugs, researchers determined that the rhythmic oscillations that drive feeding are produced by neurons in the buccal ganglion which also relay efferent motor signals

associated with these movements to the brain. Within the brain, these relay neurons directly inhibit the activity of the motor neurons responsible for the withdrawal reflex, thus preventing the slug from being startled by its own feeding movements (Kovac and Davis, 1980).

A similar set of techniques was used to delineate how the crayfish, *Procambarus clarkii*, distinguishes between self-generated and externally-generated mechanosensory stimuli during a specific kind of escape maneuver. Crayfish detect water currents using an array of mechanosensory hairs on the caudal portion of the abdomen. When a sudden stimulus is detected, these mechanosensors activate a neural pathway that triggers a rapid “tail flip” movement that propels the animal away from the perceived threat. The synapse between the mechanosensory afferents that detect the stimulus and the second-order sensory interneurons that mediate the reflex was shown to be highly susceptible to habituation (Krasne and Bryan, 1973); this, combined with the fact that the tail flip itself creates a strong self-generated mechanosensory stimulus, necessitated a mechanism to prevent repeated activation of the escape circuit in response to the animal’s subsequent movement. The neurons that prevent desensitization were found to be a group of cells located in the abdominal ganglion which are excited by tail-flip command neurons and drive presynaptic inhibition at the terminals of mechanosensory afferents at the time of the movement (Krasne and Bryan, 1973; Bryan and Krasne, 1977).

Male crickets sing to attract mates from great distances by rubbing their forewings together. This action, called stridulation, produces self-generated sounds in excess of 100 decibels. Although external sounds presented at these intensity levels are loud enough to temporarily deafen the cricket, behavioral evidence indicates that crickets are still capable of responding to the sounds of approaching predators while singing, implying the existence of a

reafference cancellation mechanism (Heiligenberg, 1969). The circuit responsible for reafference cancellation in the *Gryllus bimaculatus* cricket was identified in a set of landmark experiments by Poulet and Hedwig, who developed a method for simultaneously driving song production and recording intracellularly from auditory neurons in an intact cricket preparation (Poulet and Hedwig, 2002; James F. A. Poulet and Hedwig, 2003; J. F. A. Poulet and Hedwig, 2003). Poulet and Hedwig showed that auditory neurons responded more weakly to the cricket's own song than to externally generated sounds at the same intensity. When they stimulated the song production circuit but clipped one of the forewings to eliminate the resulting auditory stimulus, they observed inhibitory responses in auditory neurons that were locked to the movement of the intact wing, in the form of both presynaptic depolarizations at the primary auditory axon terminals and inhibitory postsynaptic potentials (IPSPs) in auditory interneurons. The precisely timed inhibition remained intact even after all other sensory nerves were cut, indicating that it originates internally in the form of an efferent motor command. In a later study, the authors identified the corollary discharge interneuron (CDI) responsible for this effect (Poulet and Hedwig, 2006). The CDI is a bilaterally paired neuron with dendrites in the mesothoracic ganglion, which contains the central pattern generators that drive wing movements during song production. The CDI is excited by these motor neurons but does not directly influence sound production itself. Using paired recordings, Poulet and Hedwig showed that the CDI spikes at exactly the time that a sound pulse is produced and is responsible for both the depolarizations seen in primary auditory afferents and the IPSPs observed in auditory interneurons during fictive singing. Together, these studies offered the first cellular-level description of reafference cancellation in the context of auditory communication. One especially interesting property of CDI neurons is that their axons innervate nearly every sensory ganglion in the central nervous

system, implying that they may function to suppress not just the auditory consequences of sound production but song-related reafference in other modalities as well, such as the mechanosensory stimuli generated by wing movement.

Beginning in the 1990s, researchers began to identify the neural pathways underlying predictive cancellation in primates. Extracellular recordings from visual neurons in the frontal eye field (FEF) and lateral intraparietal area (LIP) of rhesus macaques showed that the location of neurons' receptive fields underwent a shift before the initiation of a visual saccade (Duhamel, Colby and Goldberg, 1992; Umeno and Goldberg, 1997). These observations implied the existence of a signal that predicts the direction and intensity of an upcoming eye movement and adjusts the receptive fields of FEF and LIP neurons accordingly to preserve visual stability during the movement. In a milestone set of experiments, researchers Sommer and Wurtz identified the source of the signal as the superior colliculus, which contains neurons that are activated prior to saccadic eye movements and connects to the FEF through the mediodorsal nucleus (MD) of the thalamus. Sommer and Wurtz trained monkeys to perform a two-step visual task that required them to fixate on a starting point and then make saccades toward two targets that are flashed sequentially at different locations in the monkey's visual field. An important feature of this task is that the fixation point and the two targets are removed before the saccades begin – in other words, all eye movements are performed in the absence of visual feedback. In this scenario, the second saccade must be performed based on internal information about where the eye landed after the first saccade. By combining this behavioral task with recordings, the researchers showed that MD relay neurons encode the vector of impending eye movements, and that pharmacological disruption of the MD pathway diminished the accuracy of the second saccade (Sommer and Wurtz, 2002, 2004). Additionally, they showed that disrupting motor

signals from the MD altered the shift in the receptive fields of FEF neurons that occurs prior to eye movement (Sommer and Wurtz, 2006).

In the sensory systems discussed thus far, the reafference cancellation signals described have been derived from invariant motor-related signals. However, cancellation signals in other systems can be more complex. There are a number of examples in which reafference is predicted and canceled based on plastic signals that can accommodate changes in the properties of reafferent feedback over time.

One of the most complete cellular-level descriptions of reafference prediction and cancellation to date comes from the electrosensory system of weakly electric mormyrid fish. Weakly electric fish produce stereotyped electrical organ discharges (EODs) from an organ near the tail and detect electrosensory signals using highly sensitive electroreceptors distributed across the skin. The EOD is used in two ways: for communication, where fishes signal their behavioral state and identity to one another, and for active electrosensation, where they detect nearby objects that create distortions in their own EOD. In the electric fish literature, internally generated signals related to the act of producing an EOD are referred to as corollary discharge signals. The main experimental advantage of studying mormyrid fish is that the electromotor command neurons that produce the EOD generate a high-fidelity copy of the discharge signal even when the tail has been electrically silenced with curare. Under these conditions, researchers can deliver external waveforms that mimic the EOD while recording electrosensory responses in the brain, which is located far away from the recording site for the EOD motor command.

Mormyrid fish have three types of electroreceptive afferents that detect unique types of electrosensory signals and terminate in distinct regions of the central nervous system. The first

type, known as Knollenorgan receptors, primarily detect communication signals and terminate in the nucleus of the electrosensory lobe (nELL). The other two types, mormyromast receptors and ampullary receptors, terminate in a region known as the electrosensory lateral line lobe (ELL). Mormyromast receptors respond best to EOD signals during active sensing, whereas ampullary receptors detect weak, low-frequency changes in the surrounding electric field generated by other aquatic animals, such as prey, during passive electrosensing. The electric organ itself is comprised of specialized muscle cells whose firing pattern is determined by the electromotor command nucleus (CN). CN neurons have bifurcating axons, with one branch targeting medullary relay nucleus (MRN) neurons that project down the spinal cord to excite the electromotor neurons that produce the EOD (Bell, Libouban and Szabo, 1983). The second CN axonal branch targets a region known as the bulbar command-associated nucleus (BCA), whose target nuclei have been shown to mediate virtually all corollary discharge effects within the central electrosensory system (Bell and von der Emde, 1995; Bell *et al.*, 1995; Mohr, Roberts and Bell, 2003a, 2003b).

Several different types of corollary discharge signals originating from the CN have been shown to influence electrosensory responses during an EOD. The responses of Knollenorgan afferents, for example, are inhibited by an invariant motor-copy-like signal that prevents them from becoming desensitized by the fish's own signal, enabling the detection of external EOD signals generated by other fish (Zipser and Bennett, 1976; Bell, Libouban and Szabo, 1983; Bell and Grant, 1989). In contrast, the signals that shape mormyromast and ampullary responses in the ELL have been shown to be plastic and are updated based on the characteristics of electrosensory reafference over time. Ampullary receptors, as mentioned, are involved in detecting the low-frequency electric fields generated by prey during passive electrosensation.

Ampullary receptors respond to the fish's own EOD with a long, multiphasic response that would be masked by a strong and invariant cancellation signal like the one received by the Knollenorgan pathway. In the 1980s, Curtis Bell and colleagues devised a clever set of experiments to determine how corollary discharge signals are used to cancel these self-generated signals in the ampullary pathway without discarding behaviorally relevant signals from external sources (Bell, 1981). In those experiments, Bell recorded from units in the ampullary region of the ELL while delivering an external electrical stimulus to curarized fish that was triggered off the fish's fictive EOD command. Initially, ELL neurons responded to this stimulus with a response profile that was similar to the one evoked in primary ampullary afferents in response to the fish's own EOD. However, over repeated presentations of the same stimulus, ELL responses began to decline. When Bell uncoupled the external stimulus from the EOD command, he found that ELL neurons now responded to EOD command alone (whereas they had not before EOD-stimulus pairing), and that the shape of this response appeared to be an inverted version of their initial response to the electrical pulse stimulus. Over time, the response to the unpaired EOD command alone also diminished. These observations suggested for the first time that corollary discharge signals were being used to generate a modifiable prediction – or in Bell's words, a “negative image” – about the sensory consequences of the fish's own EOD. Later studies found that these negative images are created through spike-timing-dependent plasticity in combination with an anti-Hebbian learning rule (Bell *et al.*, 1993, 1997; Markram, Gerstner and Sjöström, 2011). More recently, a similar mechanism was shown to be involved in generating predictions about the electrosensory consequences of the fish's tail movements during active sensing, in which dynamic negative images are generated based not only on EOD commands but also on proprioceptive feedback from the tail (Requarth, Kaifosh and Sawtell, 2014).

Another example of a more sophisticated form of reafference prediction comes from the vestibular system of primates, which serves to detect head movements based on signals from vestibular organs located in the inner ear. This information is used for a variety of purposes, including directing eye movements, maintaining posture, and estimating self-motion and orientation in space. Like other sensory systems, the vestibular system must be able to distinguish self-generated stimuli resulting from voluntary head movements from externally generated stimuli arising from an outside force. In primates, afferent output from the vestibular organs converges on a region of the brain known as the vestibular nucleus, which contains two types of neurons. Neurons in the first category, known as vestibulo-ocular reflex (VOR) neurons, respond to both voluntary and externally induced head rotations in a similar way. Neurons in the second category, known as vestibular-only (VO) neurons, only carry information about externally induced rotations (Cullen 2012). The mechanism that was initially proposed to explain the more selective response profile of VO neurons was that they are directly inhibited by an efferent copy of neck motor commands during self-initiated rotations. However, the actual mechanism proved to be more interesting: VO neurons were shown to be modulated by a gated inhibitory signal that is only present when proprioceptive signals from the neck matched internal motor signals related to head motion (Roy and Cullen, 2004). These two signals were found to converge in the rostral fastigial nucleus (rFN), a region of the cerebellum that receives both proprioceptive sensory signals related to head motion as well as premotor inputs from cortical areas involved in producing neck and head movements (Brooks and Cullen, 2009, 2013; Cullen *et al.*, 2011). When the relationship between the motor command and resultant movement was altered, rFN neurons showed gradual changes in their responses, similar to the process of negative image generation seen in the electric fish (Brooks, Carriot and Cullen, 2015).

In the classic framework (von Holst and Mittelstaedt, 1950), the basis for predicting self-generated sensory signals is just the internal motor command itself. Indeed, there is evidence that motor commands can be sufficient to initiate this process: the mere act of attempting to initiate a saccade produces a prediction of the expected optic flow that will result from that eye movement, whether or not the eye actually moves at all (von Helmholtz, 1867). Motor commands are useful for generating predictions because motor commands are potentially available even before a voluntary movement begins.

However, during an ongoing movement, it would be ideal for the nervous system to also update and refine this prediction based on incoming self-generated sensory signals. A central tenet of predictive coding is that current sensory signals can be predicted, to a large degree, from sensory signals in the immediate past (Srinivasan, Laughlin and Dubs, 1982). Therefore, during an ongoing movement, the most accurate prediction should result from combining internal signals in the immediate past (motor commands or behavioral states) with self-generated sensory signals in the immediate past, in order to better predict self-generated sensory signals at the current moment (Wolpert and Ghahramani, 2000; Laurens and Angelaki, 2017). Thus, engineered systems often combine copies of commands with sensor feedback about the consequences of those commands, in order to better estimate the state of a system (Åström and Murray, 2010). There is also behavioral evidence that human subjects combine command-based predictions with sensory feedback during motor control (Johansson and Cole, 1992; Wolpert and Ghahramani, 2000). However, there is limited evidence for how this is implemented at the cellular level.

Here we describe a cell type in the *Drosophila* optic lobe (LT52) that uses a combination of internal signals and external sensory signals to detect a specific type of voluntary movement

— namely, head grooming. These cells are positioned to inhibit the visual pathways that detect external objects, and thereby to subtract predicted grooming-related visual signals from incoming visual information. Thus, LT52 cells appear to represent a mechanism for predicting and canceling self-generated visual signals in a particular behavioral context. In general terms, our findings show how the nervous system can build robust predictions about sensory experiences, based on the fusion of internal and external information.

2. Results

2.1 Experimental overview

The LT52 population consists of 15-16 neurons per hemisphere (Zheng *et al.*, 2018; Scheffer *et al.*, 2020; Dorkenwald *et al.*, 2023). The dendrites of individual LT52 neurons extend along the horizontal axis of the lobula (LO) and collectively tile the dorsal-ventral axis of the eye. They then project to the largest optic glomerulus in the central brain, the medial anterior optic tubercle (mAOTU, **Figure 1a-b**). We generated a split-Gal4 line (Luan *et al.*, 2006; Pfeiffer *et al.*, 2010) that labels roughly half of the LT52 population, approximately 7 neurons per hemisphere (**Figure 1c**). We then used this split-Gal4 line to drive GCaMP7f expression in LT52 neurons, and we used 2-photon microscopy to monitor activity in the axons of LT52 neurons in the mAOTU. Because LT52 axons are not retinotopically organized, we averaged the calcium response across the full volume of the mAOTU. The fly was surrounded by a cylindrical LED panorama that allowed us to present stationary and moving visual patterns. The fly stood on an air-supported ball that allowed it to walk freely (**Figure 1d**). In these experiments, flies typically alternated between walking and resting.

2.2 Activity during head grooming is driven by visual and non-visual input

The first thing that we noticed about LT52 neurons is that their activity was suppressed when the fly walked, whereas their activity was overall higher when the fly was not walking (**Figure 2**). Upon closer inspection, we noted that LT52 cells were activated at particular moments during resting epochs. Specifically, these large transient increases in LT52 activity coincided with moments when the fly used its forelegs to groom its head (**Figure 3a-b**).

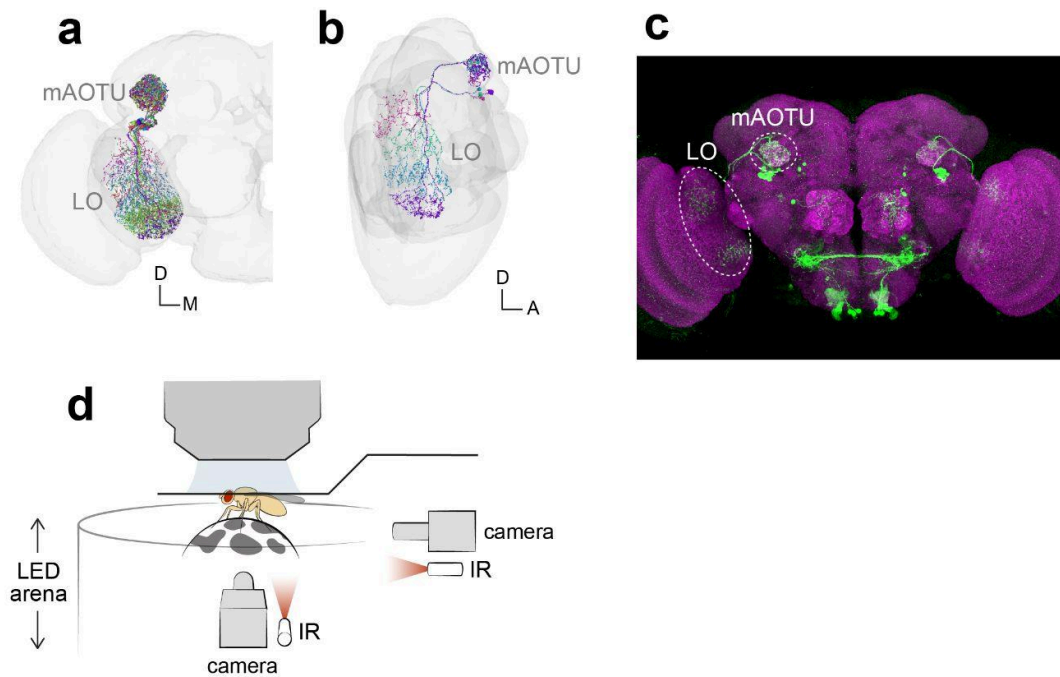


Figure 1: Imaging of LT52 activity during head grooming

(a) Anterior view of the brain showing 15 reconstructed LT52 neurons from the whole-brain connectome (Zheng *et al.*, 2018; Dorkenwald *et al.*, 2023). LT52 neurons have dendrites in the lobula (LO) region of the optic lobes and project to the medial anterior optic tubercle (mAOTU).

(b) Side view of the brain showing the dendritic morphology of 4 of the 15 LT52 neurons within the lobula. The dendrites of each individual neuron span the anterior-posterior axis of the eye. As a population, LT52 neurons tile the dorsal-ventral axis.

(c) Expression pattern of the split-Gal4 driver line used for LT52 imaging. The driver line labels approximately 7 LT52 neurons per hemisphere. Gal4-driven expression of $20\times$ UAS-mCD8::GFP (anti-GFP antibody labeling, green) and neuropil marker (anti-Brp, magenta) are shown.

(d) Schematic of experimental setup. We used 2-photon imaging to record GCaMP7f activity in the axons of LT52 neurons on one side of the brain. The fly was positioned on an air supported ball and surrounded by an LED arena that could be raised and lowered to present visual stimuli.

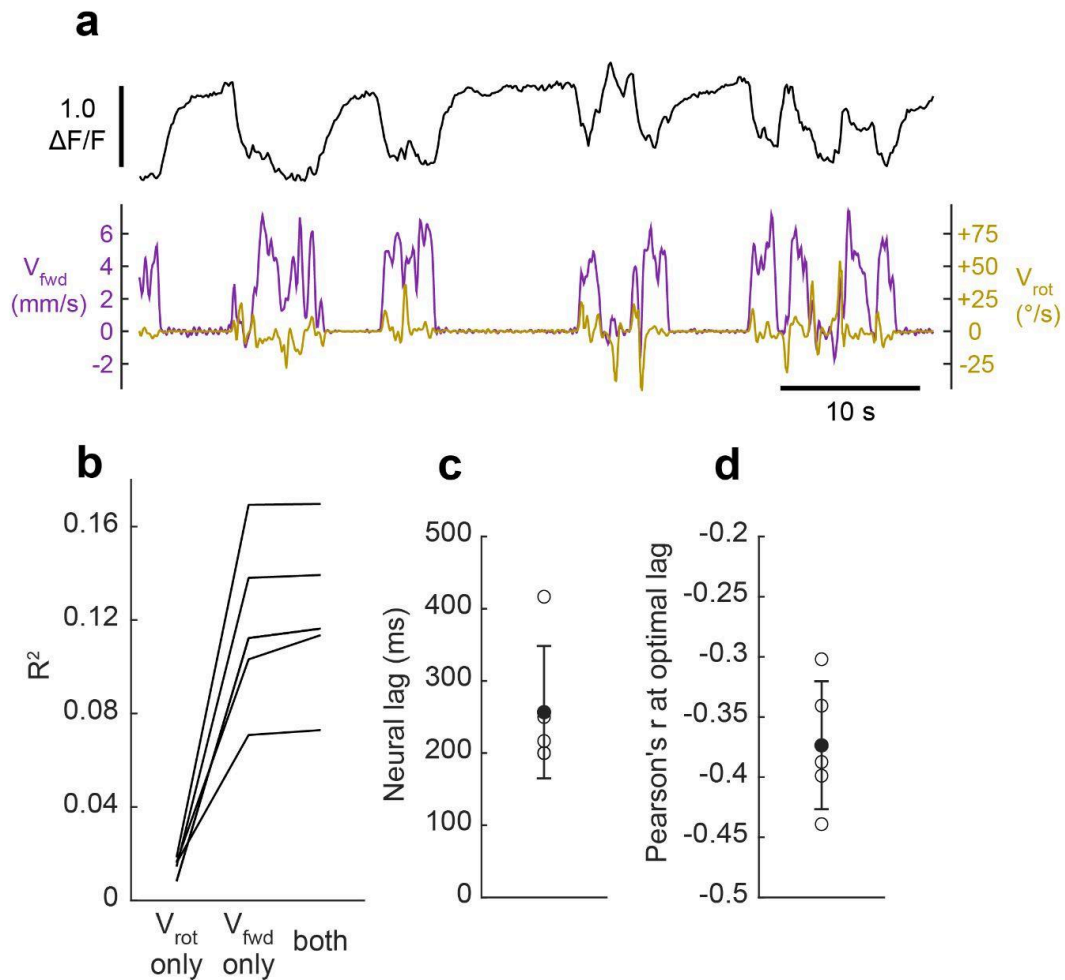


Figure 2: LT52 activity is inversely correlated with forward velocity

(a) Example trace showing inhibition of LT52 during bouts of locomotion. LT52 activity is shown in black; the fly's forward velocity (purple) and rotational velocity (gold) are shown below.

(b) Linear regression analysis using forward velocity, rotational velocity, or both variables to predict LT52 activity. We found that forward velocity was a better predictor of activity than rotational velocity. Data is from 5 minute long trials in which flies ($n=5$) walked spontaneously in the absence of a visual stimulus.

(continued on next page)

Figure 2 (continued)

(c) Cross-correlation analysis of LT52 activity and forward velocity. The left plot shows the lag that maximizes the correlation. Positive values indicate that changes in forward precede changes in LT52 activity (mean±SD = 257±92 ms, n=5 flies).

(d) Correlation coefficient (Pearson's r) at the optimal lag. Negative values indicate that LT52 activity is inversely correlated with forward velocity (mean±SD = -0.37±0.05, n=5 flies).

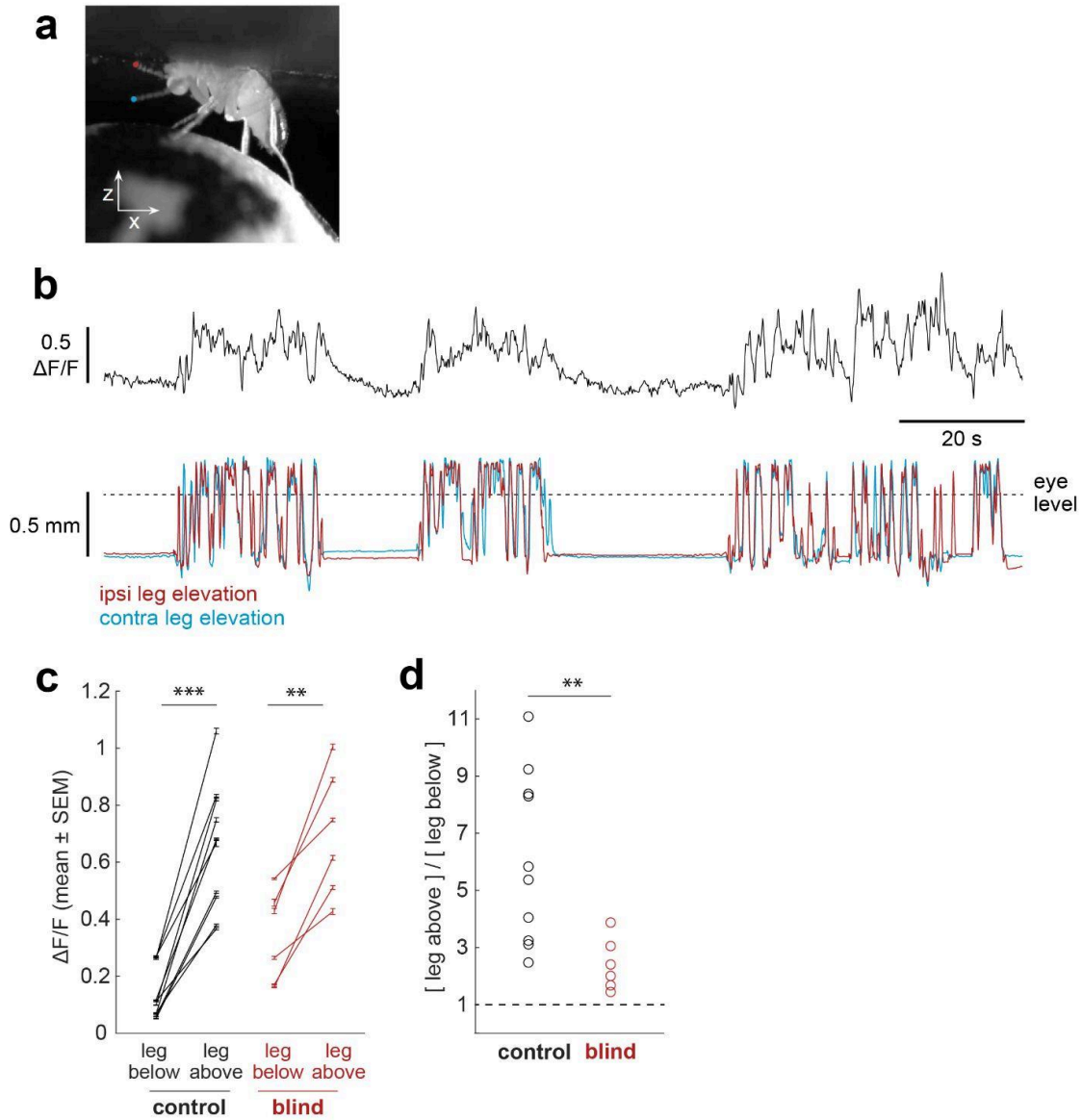


Figure 3: Activity during head grooming is driven by a combination of visual and non-visual input

(a) Side camera view of the fly. We tracked the elevation of the front leg tips (shown in blue and red) while flies groomed their heads. For these experiments the arena was illuminated at a uniform intensity and no visual stimuli were presented.

(continued on next page)

Figure 3 (continued)

(b) Example of LT52 activity during head grooming. The top trace shows LT52 fluorescence (black) and the bottom traces show the elevation of the ipsilateral and contralateral leg tips (i.e. their position in z). The dashed line marks the lowest part of the eye (“eye level”). During head grooming, flies raise their front legs off the ball and sweep them back and forth across the head, typically in synchrony.

(c) Comparison of grooming-related activity in control flies and genetically blind flies. The plot shows the mean $\Delta F/F$ when the ipsilateral leg was below or above eye level for control flies (n=10) and blind flies (n=6). Error bars show the mean \pm SEM across time points, with an average of 86 seconds of grooming (i.e. ipsilateral leg above eye level) data for each fly (range: 20-178 seconds). Activity varied significantly with the elevation of the ipsilateral leg (raised vs. lowered) (two-way analysis of variance with leg position and genotype as factors: leg position, $p=2.880e-7$; genotype, $p=0.0702$; interaction, $p=0.2499$). Post-hoc t-tests showed that activity was significantly higher when the leg was raised in both genotypes (control $p=2.492e-6$; blind $p=0.0090$). In this and subsequent figures, stars indicate significance values of $p<0.05$ (*), $p<0.01$ (**), and $p<0.001$ (***) after Bonferroni correction (where applicable).

(d) Same data as in c, but plotted as a ratio (mean $\Delta F/F$ when the ipsilateral leg was raised, divided by the mean $\Delta F/F$ when it was not). If there was no response when the leg was raised, these points would cluster around 1 (dashed line). Response ratios were significantly smaller in blind flies compared to controls (response ratio for control flies: 6.12 ± 2.98 , response ratio for blind flies: 2.35 ± 0.92 ; unpaired t-test $p=0.0099$).

Because LT52 receives the majority of its synaptic input from visual brain regions (the lobula and the anterior optic tubercle), our first thought was that LT52 must be detecting the visual image of the leg passing over the eye. However, we noticed that grooming-related activity was observable even when the fly groomed in near-darkness, when visual signals should be minimal. We therefore wondered whether these responses might be partly driven by non-visual input.

To test this idea, we imaged LT52 activity in genetically blind flies. These flies carried a null mutation in the *norpA* gene, which abolishes light-evoked photoreceptor potentials (Pak, Grossfield and Arnold, 1970; McKay *et al.*, 1995). In these blind flies, we found that LT52 neurons were still specifically active during head grooming, but their grooming responses were smaller than in genetic control flies (**Figure 3c-d**). This result demonstrates that the grooming response in LT52 neurons is driven by a combination of visual and non-visual input.

Non-visual input could arise from mechanosensory feedback during grooming, copies of leg movement commands (efference copy), or a high-level internal behavioral state signal that signals a shift from “not grooming” to “grooming.” To investigate this possibility, we examined the relationship between LT52 activity and the movement of each front leg. We found that the ipsilateral leg was a better predictor of LT52 activity than the contralateral leg, and this was true in both blind flies and genetic controls (**Figure 4a-d**). The movement of the two legs is often correlated, but if we model LT52 activity as a function of the ipsilateral leg’s position, and then we add the contralateral leg’s position as an additional predictive variable, this adds essentially no explanatory power to the model; thus, the component of LT52 activity that can be explained by leg movement is explainable on the basis of the ipsilateral leg only. This result is interesting in the case of blind flies because it indicates that the non-visual component of the response is

lateralized – i.e. LT52 activity is specifically linked to the movement of the ipsilateral leg. This finding argues that the non-visual signal is not a high-level internal state signal that represents the behavioral state of “grooming” but rather a signal that is specifically related to the movement of the ipsilateral leg. Thus, the non-visual component of LT52 activity is likely due to ipsilateral mechanosensory feedback and/or copies of ipsilateral motor commands.

These same experiments also provided evidence that the non-visual component is faster than the visual component. Specifically, we found that blind flies and control flies had the same fast uptick in LT52 activity just after grooming onset, but in control flies, LT52 activity continued to rise more slowly for several hundred milliseconds thereafter, whereas in blind flies this additional slow rise was absent. This result implies that the non-visual component is fast, whereas the non-visual component is slower (**Figure 4e**). We also performed a complementary analysis where we computed the time lag that maximized the correlation between ipsilateral leg position and LT52 activity. We found that the lag was shorter for genetically blind flies compared to controls (**Figure 4f**). Taken together, these observations support the idea that grooming responses in LT52 neurons are driven by fast non-visual signals followed by slower visual signals.

If LT52 grooming responses are primarily driven by sensory feedback from the ipsilateral leg, then they should be reduced if the ipsilateral leg is prevented from grooming. Indeed, we found that responses decreased after we removed most of the ipsilateral leg, leaving only a short stump (**Figure 5a-c**). Some responses remained after stumping, and this may be due to motor efference copy, which would likely remain intact after stumping, or else residual proprioceptive or visual signals from the stump.

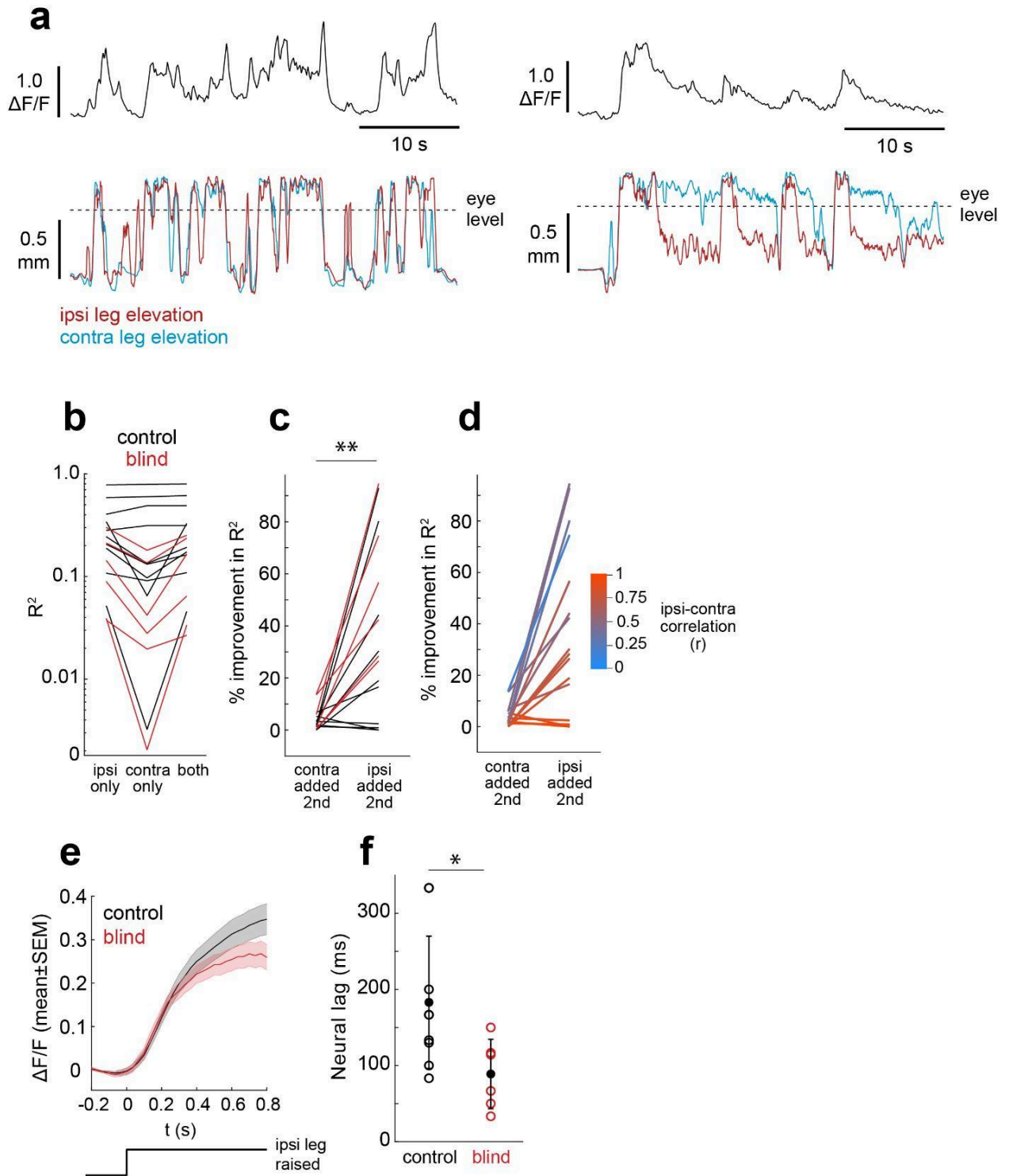


Figure 4: The ipsilateral leg is a better predictor of LT52 activity

(continued on next page)

Figure 4 (continued)

(a) Example traces showing LT52 activity when the fly raised its front legs synchronously (left) and asynchronously (right). $\Delta F/F$ is shown in black and the elevation of the ipsilateral and contralateral legs are shown in red and blue. Flies typically raised their front legs in synchrony (as shown by the overlapping red and blue traces in the left plot), making it difficult to tell whether activity was better correlated with one leg versus the other. However, when the legs moved independently (as in the right plot), LT52 activity tracked with the elevation of the ipsilateral leg.

(b) Predictive power of a linear model using only the ipsilateral leg, only the contralateral leg, or both legs as variables (n=10 control flies, n=6 blind flies).

(c) Improvement in R^2 gained by adding the contralateral or ipsilateral leg to a model with both legs as variables. Adding the ipsilateral leg to the model yielded a bigger improvement in R^2 than adding the contralateral leg to the model (R^2 , contra added second: $4.22 \pm 4.86\%$, R^2 , ipsi added second: $36.40 \pm 32.32\%$, paired t-test, $p=0.001$, n=16 flies).

(d) Same data as c, but color-coded to show the correlation between the ipsilateral and contralateral legs (Pearson's r). The difference in predictive power was most evident when the legs were less correlated.

(e) LT52 responses at the time of leg elevation. Traces show the mean \pm SEM across n=216 events in control flies and n=117 events in blind flies.

(f) Cross-correlation analysis showing the lag that maximizes the correlation between $\Delta F/F$ and ipsilateral leg position in control and blind flies. Positive values indicate that changes in leg elevation precede changes in $\Delta F/F$. The optimal lag was significantly shorter for blind flies compared to controls (control flies, n=10: 183 ± 87 ms, blind flies, n=6: 89 ± 46 ms, unpaired t-test, $p=0.0289$).

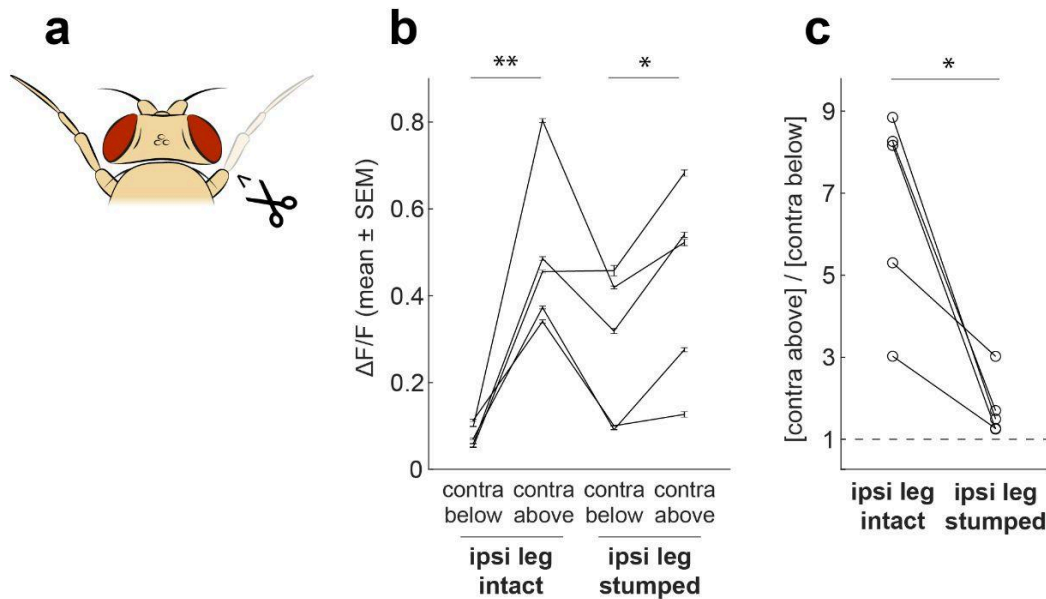


Figure 5: LT52 responses are reduced but not abolished when the ipsilateral leg is stumped

(a) We imaged LT52 activity before and after removing most of the ipsilateral leg, leaving only a short stump intact.

(b) Comparison of grooming-related activity before and after the ipsilateral leg was stumped ($n=5$ flies). For this analysis we used the position of the contralateral leg as a proxy for when the ipsilateral leg was raised, because it was difficult to track the stump's position. Activity varied significantly with the position of the contralateral leg (two-way analysis of variance with contralateral leg position and ipsilateral leg intact/stumped as factors: leg position, $p=0.0018$; leg intact/stumped: $p=0.3802$; interaction, $p=0.1043$). Post-hoc t-tests showed that activity was significantly higher when the contralateral leg was raised, and this was true regardless of whether the ipsilateral leg was stumped (leg intact: $p=0.0070$; leg stumped: $p=0.0165$). Error bars show the mean \pm SEM across time points, with an average of 89 seconds of grooming data (i.e. contralateral leg raised above eye level) for each fly (range: 17-144 seconds).

(c) Same data as in b, but plotted as a ratio (mean $\Delta F/F$ when the contralateral leg was raised, divided by the mean $\Delta F/F$ when it was lowered). Response ratios were significantly smaller after the ipsilateral leg was stumped (response ratio with leg intact: 6.70 ± 2.48 , response ratio with leg stumped: 1.74 ± 0.74 ; paired t-test $p=0.0149$).

We left the stump intact in these experiments because it allowed us to verify that the stump continued to move in a manner that was roughly correlated with the grooming movements of the contralateral (intact) leg; this shows that ipsilateral leg commands were still being generated after stumping. In short, this experiment provides further support for the conclusion that LT52 responses are due — at least in part — to sensory feedback from the ipsilateral leg during grooming.

2.3 Visual tuning of LT52 matches leg movements during grooming

Thus far, we have seen that LT52 cells respond to grooming and these responses are partly visual in origin. But when the fly grooms, what does the eye actually see? And does this match the visual tuning of LT52? To investigate this question, we first analyzed the movement of the tibia, the leg segment that moves back and forth across the eye during grooming, within the constraints of our fly holder (**Figure 6a-b**). When the tibia is moving in front of the eye, it should appear as a dark moving stripe. We estimated the width of the tibia to be approximately 32° of visual space when the tibia is positioned directly in front of the eye. We found that, when the fly is grooming its head, the angle of the tibia is generally positioned $40\text{-}80^\circ$ from vertical (**Figure 6c**). During a grooming bout, the tibia sweeps back and forth across the eye at a wide range of speeds, including speeds in excess of several hundred degrees per second (**Figure 6d-f**). A spectral analysis of these sweeping movements indicated that their dominant frequency was approximately 7.5 Hz (**Figure 6g-h**).

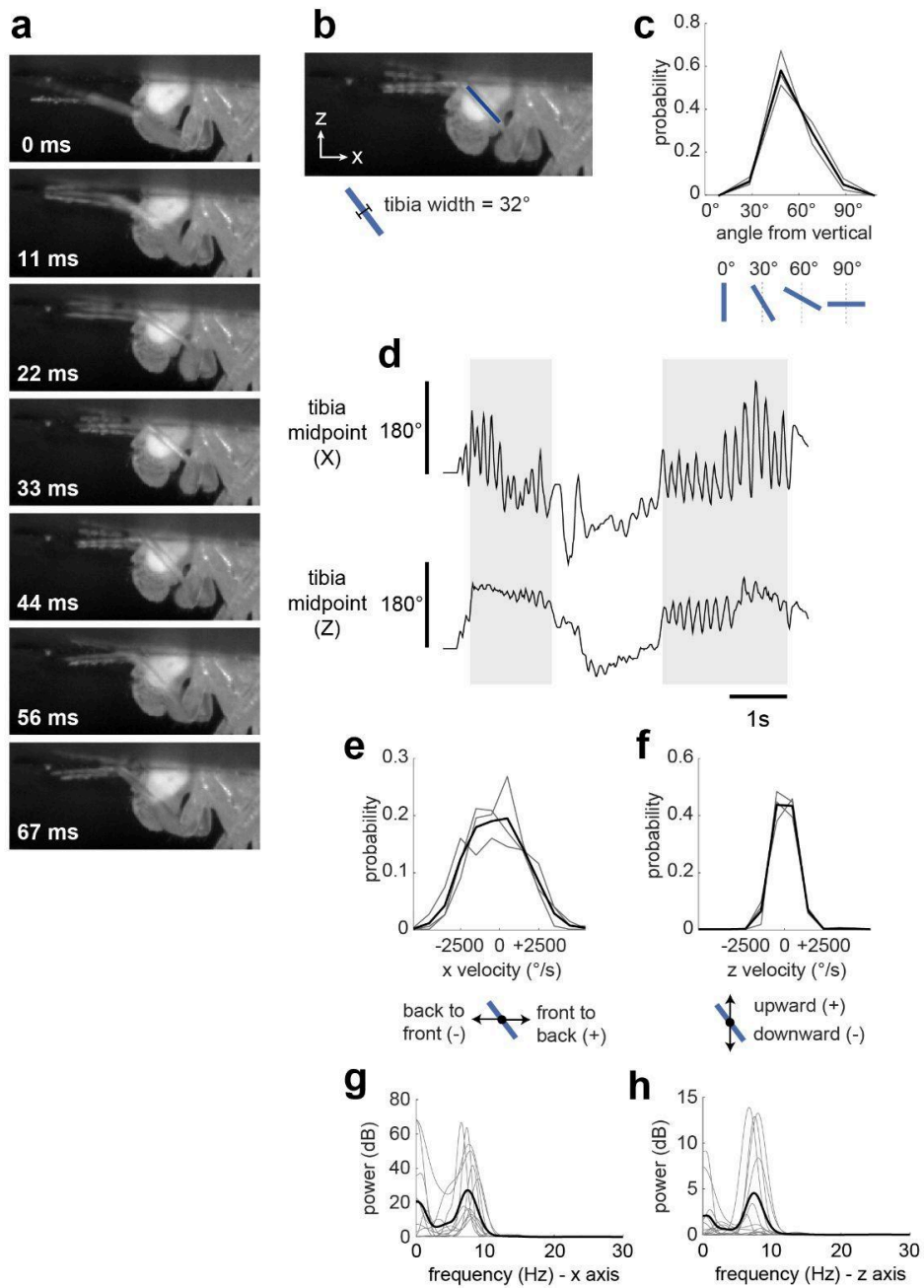


Figure 6: Leg movements during head grooming

(a) Sequence of frames showing the movement of the leg during head grooming. During grooming, the leg sweeps backwards and upwards towards the posterior part of the head and then returns to the anterior part of the head. The fly repeats this cycle many times for up to several seconds before it lowers its legs. Video was acquired at a frame rate of 90 Hz.

(continued on next page)

Figure 6 (continued)

(b) The tibia (shown in blue) is the leg segment that is most visible to the eye during head grooming. The width of the tibia is approximately 32° of visual space. See Methods for details.

(c) Histogram showing the angle of the tibia during head grooming. Tibia angle is measured relative vertical, as shown in the schematic below the plot. Gray lines show the distribution of angles for each of 3 flies, with 3-7s of grooming data per fly. The black line shows the average across flies (mean \pm SD = $56.2\pm 13.1^\circ$).

(d) Example traces showing the position of the tibia midpoint on the x and z axis. Axes are shown in panel b. Gray shading indicates the periods of tibia movement that we analyzed as bouts of head grooming, defined as times when the tarsus-tibia joint was above eye level. The position of the tibia midpoint has been converted from millimeters to degrees based on the assumption that each eye subtends approximately 180° of visual space on the horizontal axis.

(e) Histogram showing the velocity of the tibia midpoint on the x axis during head grooming bouts (n=3 flies, with 3-7s of grooming data per fly). Same plotting convention as the histogram in panel c. Positive velocities indicate movement in the front-to-back direction (i.e., anterior to posterior); negative velocities indicate movement in the back-to-front direction. Mean \pm SD of mean distribution = $-218\pm 1785^\circ/\text{s}$.

(f) Same as panel e, but showing the velocity of the tibia midpoint on the z axis. Positive velocities indicate movement in the upward direction (i.e., ventral to dorsal); negative velocities indicate movement in the downward direction. Mean \pm SD of mean distribution = $-56\pm 674^\circ/\text{s}$.

(g) Frequency analysis of tibia movement on the x axis. Each gray line shows the power spectrum for a sustained period of head grooming $>1\text{s}$ in duration (n=11 bouts from 3 flies). The black line shows the mean power distribution, with a peak at 7.51 Hz.

(h) Same as panel g, but for tibia movement on the z axis. The peak of the mean distribution is 7.42 Hz.

We then investigated the visual tuning properties of LT52 neurons. For these experiments, we first removed the fly's ipsilateral leg to minimize visual signals related to head grooming and then raised the LED arena to present visual stimuli. We first presented the fly with a drifting vertical grating moving front-to-back at various speeds. LT52 cells were robustly activated by a wide range of speeds, including speeds of several hundred degrees per second (**Figure 7a-b**). When we varied both speed and spatial frequency, we found that LT52 responses were dependent on the interaction of these parameters, in a manner indicating that these cells favor high temporal frequencies close to 7 Hz (**Figure 7c-d**). Together, these data imply that LT52 is well-suited to detect the range of leg movement speeds and temporal frequencies seen during grooming bouts.

LT52 neurons were also strongly directional, with stronger responses to front-to-back movement, as compared to back-to-front movement. This implies that the front-to-back sweeps during grooming provide the primary visual stimulus to these neurons (**Figure 7e**). Interestingly, LT52 neurons also responded to upward movement of a horizontal grating, suggesting that they are also detecting some of the leg's upward movement.

Next, we tried presenting front-to-back movement to each visual hemifield alone (**Figure 7f**). We found that LT52 neurons were strongly activated by movement in the ipsilateral hemifield, but not the contralateral hemifield. This is consistent with our finding that LT52 neurons are primarily correlated with the movement of the ipsilateral leg, not the contralateral leg (Figures 4 and 5).

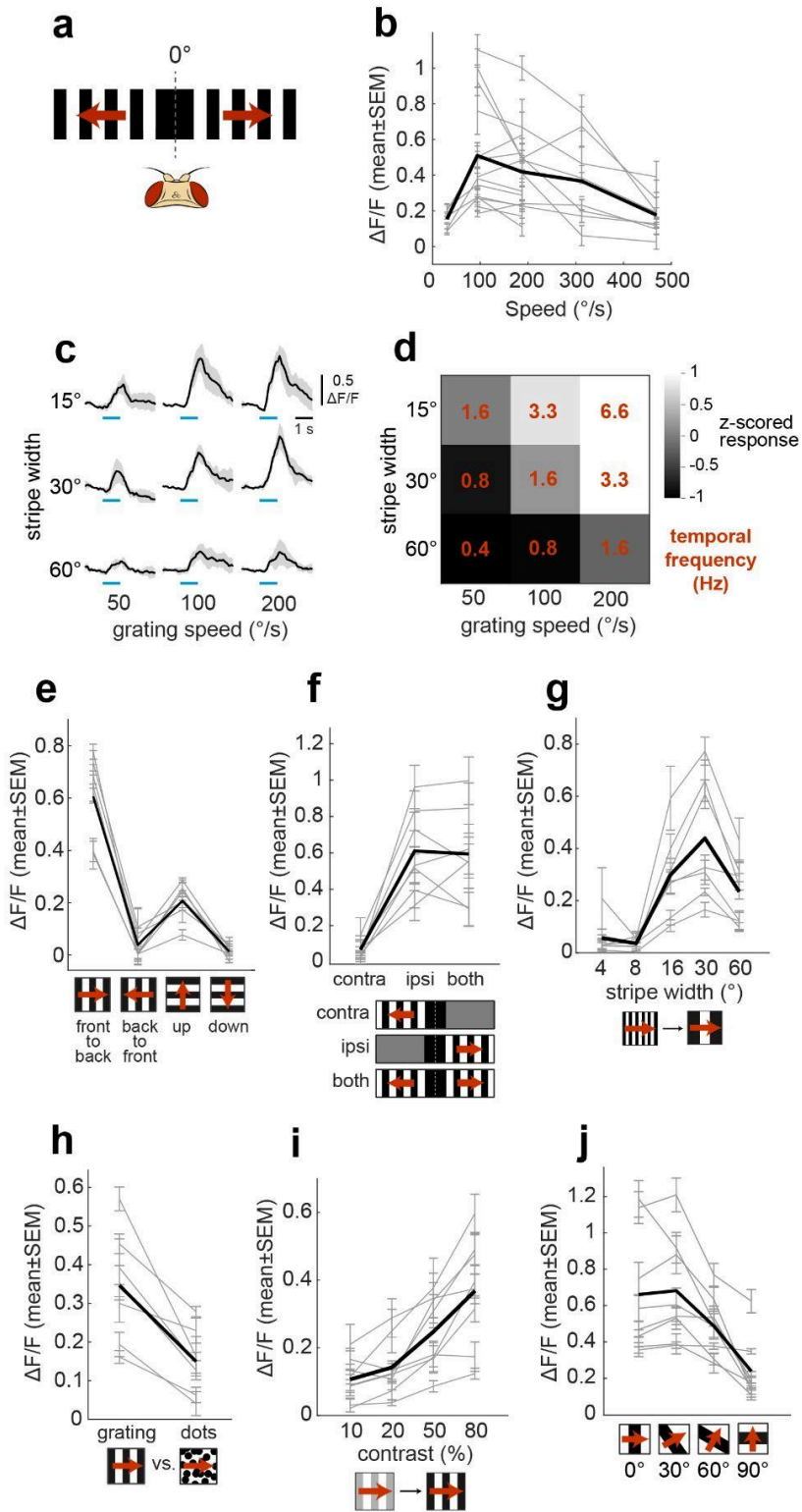


Figure 7: Visual tuning properties of LT52

(continued on next page)

Figure 7 (continued)

(a) Schematic of stimulus presentation. Red arrows indicate the direction of motion of the pattern and 0° marks the visual midline. All visual stimuli were mirrored across the midline so that both eyes experienced stimulus motion in the same direction – e.g, a vertical grating moving in the front-to-back direction, as illustrated. The region directly in front of the fly ($\pm 15^\circ$) was blanked out so that patterns with vertical bars did not appear to be expanding or retracting from the visual midline.

(b) LT52 responses to a vertical grating moving in the front-to-back direction at different speeds. Gray lines show the responses of individual flies. The black line shows the average across flies ($n=7-15$ flies for each speed tested). Note that not all speeds were tested in every fly. The values plotted are the peak $\Delta F/F$ response in a 2s window following stimulus onset (mean \pm SEM across 15 stimulus repetitions). Grating parameters: speed: variable, stripe width: 16° , contrast: 100%.

(c) Temporal frequency tuning plot for an example fly, showing the trial-averaged response to a vertical grating moving in the front-to-back direction. We varied the speed of movement and width of the stripes in the grating as indicated on the x and y axes.

(d) Heatmap of LT52 responses to the stimulus combinations described in c. Gray shades show the z-scored response to each stimulus, averaged across $n=7$ flies. The temporal frequency of each stimulus is shown by the red numbers.

(e) Responses to grating motion in four different directions. LT52 neurons were imaged on the right side of the brain and the red arrows in the stimulus icons indicate the direction of motion in the right visual field. Gray lines show the responses of individual flies. The thick black line shows the mean across flies ($n=7$). Grating parameters: speed of motion: $120^\circ/s$, stripe width: 16° , contrast: 100%.

(f) LT52 responses to vertical gratings moving in the front-to-back direction. The grating was presented in the contralateral visual field, the ipsilateral visual field, or both hemifields. Grating parameters: speed of motion: $120^\circ/s$, stripe width: 16° , grating contrast: 100%.

(g) LT52 responses to a grating moving in the front-to-back direction at a fixed speed with different stripe widths. Gray lines show the responses of individual flies. The black line shows the average across flies ($n=7$). Grating parameters: speed: $120^\circ/s$, stripe width: variable, contrast: 100%.

(continued on next page)

Figure 7 (continued)

(h) Responses to a vertical grating compared to a random polka dot pattern. The diameter of the dots was equal to the width of the stripes in the grating and the two patterns were matched in terms of overall luminance. Gray lines show the responses of individual flies. Black lines show the mean across flies (n=7). Stimulus parameters: speed: $120^\circ/\text{s}$, stripe width and spot diameter: 16° , contrast: 100%.

(i) LT52 responses to a grating moving in the front-to-back direction with different contrasts. Gray lines show the responses of individual flies. The black line shows the average across flies (n=8). Stimulus parameters: speed: $120^\circ/\text{s}$, stripe width: 16° , contrast: varies.

(j) Responses to a “leg like” stimulus consisting of a single 30° wide bar moving in the front-to-back and upward direction, orthogonal to angles occupied by the tibia during head grooming. The orientation of the bar ranged from 0° (i.e. a vertical bar moving front-to-back) and 90° (a horizontal bar moving upward). The bar moved at a speed of $470^\circ/\text{s}$.

Next, we examined the response to vertical gratings moving in the front-to-back direction while we varied the width of the vertical stripes in the visual pattern. For gratings moving at a fixed speed, we found that a stripe width of 30° was the best stimulus (**Figure 7g**). Thus, the spatial frequency tuning of LT52 neurons is well matched to the estimated size of the leg's image during grooming. We also found that a pattern of dense random dots was a poorer stimulus for LT52 than a vertical grating, even when the stimuli were matched in terms of spatial frequency and contrast (**Figure 7h**). This result implies that LT52 neurons preferentially respond to extended visual edges. Increasing the contrast of the vertical grating produced a graded increase in the neural response, as we might expect (**Figure 7i**).

Finally, to confirm that LT52 responds to a stimulus with the leg movement parameters seen during grooming, we presented flies with a “leg-like” stimulus consisting of a single 30° wide bar that moved in the front-to-back and upward direction, orthogonal to the angles occupied by the tibia during head grooming sweeps (**Figure 6c**). We found that LT52 responded strongly to this stimulus. As we would expect based on the direction selectivity of LT52 along the horizontal and vertical axes, we found that responses were strongest when the bar was oriented vertically and moving in the front-to-back direction and weaker when it was oriented horizontally and moving upwards.

In summary, the visual tuning properties of LT52 are well-matched to detect the leg movements that occur during head grooming. LT52 primarily responds to extended visual edges with a leg-like spatial frequency, speed, and temporal frequency. Together, these results support the conclusion that LT52 functions to detect the visual stimuli that result from head grooming.

3. Discussion

In this study, we identified a cell type in the *Drosophila* visual system that is specifically recruited when the ipsilateral leg is used to groom the head. Grooming responses in LT52 cells are based on a combination of visual signals and internal non-visual signals. LT52 cells are likely to be inhibitory, based on their neurotransmitter profile, and they are presynaptic to pathways that detect visual object motion. Together, all these observations imply that LT52 cells function to predict and cancel self-generated visual signals during grooming. LT52 cells reside in the lobula, where diverse cell types are tuned to detect different visual features, such as looming or translating objects of varying sizes and speeds (Otsuna and Ito, 2006; Wu *et al.*, 2016; Keleş and Frye, 2017; Ribeiro *et al.*, 2018; Morimoto *et al.*, 2020; Hindmarsh Sten *et al.*, 2021; Klapoetke *et al.*, 2022; Turner *et al.*, 2022; Schretter *et al.*, 2024). Our study provides evidence that lobula cells can be tuned to detect specific non-visual features, as well as visual features — specifically, they can be tuned to detect the organism’s own gestures.

What is the origin of the internal non-visual signals in LT52 cells? In genetically blind flies, we found that the non-visual grooming response was specifically linked to ipsilateral foreleg movement, and rather than being linked to the movement of both legs. This argues that the non-visual grooming response is not an abstract internal state signal that represents the behavioral state of simply “grooming.” Rather, this result implies that LT52 receives proprioceptive feedback, and/or a copy of a motor command which is sent to the ipsilateral foreleg. In flies where the leg was stumped, we found that grooming responses were reduced by about as much as they were in blind flies, and stumping should dramatically reduce proprioceptive feedback from the leg. The fact that such a substantial grooming response remains after stumping suggests that the non-visual input to LT52 is at least partly due to motor

commands, as we know that the motor command remains intact after stumping, because we can observe the stump moving when the fly grooms. On the other hand, there is also reason to think that non-visual signals in LT52 include proprioceptive feedback, because LT52 grooming responses tend to lag the leg's movement even in blind flies. In principle, feedback might arise mechanosensory bristles on the eyes or head, but we did not find any obvious pathway to LT52 neurons from the region of the subesophageal zone where these mechanosensory bristles terminate (Hampel *et al.*, 2017; Eichler *et al.*, 2023), and so leg proprioceptors would seem to be better candidates (Tuthill and Wilson, 2016). In short, our data suggest that LT52 grooming responses are driven by some combination of motor commands and proprioceptive signals, as well as visual signals.

In the future, it will be interesting to look for input to LT52 from the ventral nerve cord, the insect analog of the spinal cord. Input from leg proprioceptors would necessarily originate in the ventral nerve cord. Motor efference copy might also come from the ventral nerve cord, as this structure is likely to contain the central pattern generators that produce fast repetitive foreleg movements during grooming. In examining the whole-brain connectome (Dorkenwald *et al.*, 2023), we noticed that the anatomically strongest, non-visual connections onto LT52 cells arise from putative cholinergic neurons whose dendrites reside in the posterior lateral protocerebrum (PLP), and whose axons project to the lobula (LO). These cells, which are known as cLLPM02, receive strong anatomical input from ascending axons from the ventral cord. The anatomy of this pathway suggests it is a major source of non-visual inputs to LT52, and when a brain-and-cord connectome is available, it should be possible to identify the sources of these signals in the ventral nerve cord.

What about the visual inputs to LT52? These are clearly important, as LT52 grooming responses are significantly smaller in genetically blind flies. Overall, we found that the visual tuning of LT52 is well-matched to the leg's appearance during head grooming. Specifically, they respond to the speeds and temporal frequencies that are characteristic of leg movements during grooming. They are also tuned to the spatial frequency that matches the leg's apparent size, as well as the angles adopted by the leg during head grooming. The visual input to LT52 is strictly ipsilateral; it is notable that the non-visual input to this cell is also mainly or exclusively ipsilateral, again reinforcing the point that this cell is specifically anticipating the grooming-related visual input to one eye. Visual input to LT52 comes from several cell types in the medulla (Dorkenwald *et al.*, 2023), but these cell types have not yet been functionally characterized.

Connectome data (Zheng *et al.*, 2018; Scheffer *et al.*, 2020; Dorkenwald *et al.*, 2023) show that the main target of LT52 in the central brain is the LC10 cell type (Otsuna and Ito, 2006; Panser *et al.*, 2016; Wu *et al.*, 2016). Specifically, LT52 axons are positioned to inhibit LC10 axon terminals. LC10 cells detect small moving objects, and they guide steering toward other flies during courtship and aggression (Ribeiro *et al.*, 2018; Schretter *et al.*, 2020, 2024; Hindmarsh Sten *et al.*, 2021). Interestingly, the dendrites of the LC10 cells respond to a wide range of object speeds (up to about 300°/s), whereas the axons of LC10 cells respond mainly to slow object speeds, below about 100°/s (Ribeiro *et al.*, 2018). This comparison suggests there is some mechanism that narrows the speed tuning of LC10 axon terminals. This is particularly interesting, given that LC10 cells have a clear role in guiding male pursuit toward a female during courtship, and the image of the female tends to be relatively slow-moving (<100°/s) during courtship pursuit (Ribeiro *et al.*, 2018; Schretter *et al.*, 2024). Thus, the mechanism that

narrows the tuning of LC10 axons seems to be well-matched to the statistics of ethologically relevant target images. Here we show that LT52 cells respond preferentially to speeds in the range of about 100-300°/s; hence, LT52 cells are appropriately tuned to suppress LC10 responses to fast-moving objects.

It is also interesting to compare the direction selectivity of LC10 and LT52. LC10 responds primarily to front-to-back motion (Ribeiro *et al.*, 2018; Hindmarsh Sten *et al.*, 2021), and we found that the same is true of LT52. During head grooming, the leg rapidly alternates between the two directions of movement (back-to-front as well as front-to-back), so a visual neuron that is sensitive to either direction should be robustly activated during a grooming bout. And, if we imagine that LT52 cells function to suppress “inappropriate” visual responses in LC10 during grooming, then it might make sense for LT52 to adopt the same direction-selectivity that LC10 has. From this perspective, LT52 is not so much detecting grooming *per se* as it is detecting the features of self-generated visual signals that need to be subtracted from postsynaptic responses.

To summarize: when a fly is pursuing a moving target, such as another fly, its task is to keep the image of the target centered on its frontal visual field. When the target slips off the midline to the right, creating front-to-back motion in the right visual field, LC10 cells are activated in the right optic lobe, driving a rightward turn that reorients the body toward the object (Ribeiro *et al.*, 2018; Hindmarsh Sten *et al.*, 2021; Schretter *et al.*, 2024). However, this visuomotor response is maladaptive if the fly is grooming, because here front-to-back motion is caused by the movement of its own leg over its eye. We propose that LT52 functions to suppress this maladaptive behavior, by inhibiting LC10 axon terminals whenever there is internal and external evidence of grooming. Flies groom for a large fraction of their waking life (Qiao *et al.*,

2018), and grooming should generate a predictable set of self-generated sensory signals (Hampel *et al.*, 2015); thus, in hindsight, it is perhaps not surprising to find a cell in the visual system which is specialized for this task.

Beyond grooming, LT52 might serve the same function in any situation where foreleg movement creates a visual distraction; for instance, when flies reach across a gap in the terrain (Pick and Strauss, 2005), or when flies aggressively strike each other with their forelegs (Chen *et al.*, 2002; Zwarts, Versteven and Callaerts, 2012; Fernandez, Trannoy and Certel, 2023). More generally, LT52 might function to suppress LC10 responses to very small and fast-moving objects, whether or not they occur during foreleg movement, as these objects are unlikely to be ethologically relevant targets for pursuit. In the future, it will be interesting to test these predictions by examining the effect of silencing LT52 cells in different behavioral contexts. It would also be interesting to compare dendritic and axonal LC10 responses to leg movements in different contexts.

Broadly speaking, a basic task of the nervous system is to separate self-generated sensory signals from externally-generated sensory signals (Cullen, 2004). There are many ways to do this. In their original formulation of this concept, von Holst and Mittelstaedt (1950) proposed that motor commands should be used to predict self-generated sensory signals. However, predictions based on motor commands alone are not robust to the factors that produce unpredictable variations in motor output, such as fatigue. For this reason, a better strategy would be to combine recent motor commands with recent sensory feedback, in order to better predict current self-generated sensory signals (Wolpert and Ghahramani, 2000; Laurens and Angelaki, 2017). Then, these predictions could be used for the cancellation of self-generated signals. Although this is not the “classical” strategy suggested by von Holst and Mittelstaedt, there is

evidence that it does occur. One example is the primate vestibular nucleus, where motor commands are combined with signals from neck proprioceptors to estimate and cancel the vestibular signals arising from self-generated head rotations (Roy and Cullen, 2004). Another example is the electrosensory lobe of mormyrid fish, where motor commands are combined with signals from tail proprioceptors to estimate and cancel the electrosensory signals arising from self-generated electric field discharge (Requarth, Kaifosh and Sawtell, 2014). More recently, a study of the mouse dorsal cochlear nucleus suggested that motor commands might be combined with somatosensory signals to estimate and cancel the auditory signals arising from licking (Singla *et al.*, 2017). Our work provides another example of prediction based on the integration of internal and external signals. The example of LT52 cells is interesting because it involves vision, and vision is notably slow, as compared to mechanosensory modalities like proprioception and somatosensation (Dickinson and Muijres, 2016). Notably, we found that the visual component of the LT52 grooming response is slower than the non-visual component. This suggests that LT52 initially constructs a prediction based on fast internal sources of information (proprioception and/or motor commands), and this prediction is subsequently refined by slower visual feedback.

If LT52 cells are tuned to a specific gesture (ipsilateral leg movement during grooming), then could other cells in the optic lobe be turned to other gestures? Recent studies have also identified locomotor-related signals throughout the optic lobe (Turner *et al.*, 2022; Aimon *et al.*, 2023; Brezovec *et al.*, 2024), and these locomotor signals can function to predict and cancel self-generated visual motion during walking (Fujiwara *et al.*, 2017; Strother *et al.*, 2018; Cruz, Pérez and Chiappe, 2021; Fujiwara, Brotas and Chiappe, 2022) as well as flight (Kim, Fitzgerald and Maimon, 2015; Kim *et al.*, 2017; Fenk, Kim and Maimon, 2021). Our results argue that

ascending motor signals may be integrated with visual information in order to generate this prediction. In other words, visuo-motor integration occurs at the level of prediction, and not just cancellation. Moreover, our results show that predictions can be quite specific for particular kinematic features of movement — namely, front-to-back movements of the ipsilateral foreleg sweeping across the head.

Finally, our findings also indicate that LT52 cells are modulated by behavioral state. Specifically, LT52 cells are consistently less active when the fly locomotes, and more active when locomotion is stopped. Flies must stop to groom, and so this behavioral state modulation is consistent with the idea that LT52 specializes in detecting grooming. Interestingly, other cells generally have the opposite pattern: most of the brain is more active when the fly locomotes, and less active when locomotion is stopped (Turner *et al.*, 2022; Aimon *et al.*, 2023; Schaffer *et al.*, 2023; Brezovec *et al.*, 2024). In the future, it will be interesting to investigate how these behavioral state modulations activate some cells while suppressing others, thereby coordinating brain-wide transitions in sensation, cognition, and action.

4. Methods

4.1 Acknowledgements

We thank Kristen Branson and Alice Robie for sharing Animal Part Tracker software. We are grateful to Ofer Mazor and Pavel Gorelik of the Harvard Medical School Instrumentation Core Facility for constructing the visual display apparatus, based on designs contributed by Michael Reiser. Tom Clandinin generously donated w^+ , *norpA*[*P24*] flies. We thank the Princeton FlyWire team and members of the Murthy and Seung labs, as well as members of the Allen Institute for Brain Science, for development and maintenance of FlyWire (supported by BRAIN Initiative grants MH117815 and NS126935 to Murthy and Seung). We also acknowledge members of the Princeton FlyWire team and the FlyWire consortium for neuron proofreading and annotation. This work was supported by a grant from the NIH (U19NS104655) as well as HHMI Investigator funding to Rachel I. Wilson.

4.2 Fly husbandry and genotypes

Flies were raised on standard cornmeal-molasses food (recipe B2, Archon Scientific) in an incubator on a 12-hour/12-hour light/dark cycle at 25°C with humidity between 50-70%.

Genotypes of experimental flies are as follows:

Control flies: w^+ ; *R94E06.AD*/+ ; *R29F02.DBD*/*20x-UAS-GCaMP7f*

Blind flies: w^+ , *norpA*[*P24*] ; *R94E06.AD*/+ ; *R29F02.DBD*/*20x-UAS-GCaMP7f*

The following stocks were obtained from the Bloomington Drosophila Stock Center (BDSC):

P{*y*[+*t7.7*] *w*[+*mC*]=*R94E06-p65.AD*}*attP40* (BDSC #68698), *P*{*y*[+*t7.7*]

w[+*mC*]=*R29F02-GAL4.DBD*}*attP2* (BDSC #68751), *P**Bac*{*y*[+*mDint2*]

w⁺[+mC]=20XUAS-IVS-jGCaMP7s;VK00005 (BDSC #79032). *w⁺*, *norpA[P24]* flies were a gift from Tom Clandinin.

4.3 Fly preparation and dissection

All experiments were performed on 4-5 day old male flies. After eclosion, flies were housed individually on cornmeal-molasses food in the same incubator in which they were raised. Flies were briefly anesthetized on ice prior to dissection. The fly holder consisted of a flat sheet of titanium foil secured within a 3D-printed platform (Mars 3 Pro printer with ABS-like resin, Elegoo). The bottom of the foil was painted black to minimize reflections (Ultra-flat Black 900, Tough Guy). The fly's head was pitched in a natural, upright position with approximately three-quarters of the eye below the foil. The fly was secured in the holder using UV-curable glue (Loctite AA-3972) and cured with a brief (<1 s) pulse of ultraviolet light (LED-200, Electro-Lite Co.). To reduce brain movement, muscle 16 (Miller and Demerec, 1950) was removed and the proboscis was glued in place. After covering the dorsal surface of the head in saline, a hole was cut in the head capsule and tracheae were removed as necessary to expose the mAOTU near the dorsal surface of the brain. The external saline solution contained (in mM): 103 NaCl, 3 KCl, 5 N-tris(hydroxymethyl) methyl-2-aminoethane-sulfonic acid, 8 trehalose, 10 glucose, 26 NaHCO₃, 1 NaH₂PO₄, 1.5 CaCl₂ and 4 MgCl₂, with osmolarity adjusted to 270–273 mOsm. The solution was bubbled with 95% O₂ and 5% CO₂ and reached a pH of approximately 7.3. External solution was continuously perfused over the brain during dissection prior to imaging.

4.4 Two-photon calcium imaging

Imaging experiments were performed using a two-photon microscope with a movable stage (Thorlabs Bergamo II) and a fast piezoelectric objective scanner (Physik Instrumente P725)

for volumetric imaging. For two-photon excitation of GCaMP we used a Chameleon Vision-S Ti-Sapphire femtosecond laser tuned to 940 nm. Images were collected using a 20×/0.95 NA objective (Olympus). Emission fluorescence was collected on a GaAsP photomultiplier tube (Hamamatsu) through a 525-nm bandpass filter (Thorlabs). We used ScanImage 2018 software (Vidrio Technologies) and custom Matlab scripts to control the microscope. Imaging data was collected using National Instruments PXIe-6341 hardware. The imaging region was 256×128 pixels with 6 slices in the Z-axis for each volume (5-7 $\mu\text{m}/\text{slice}$), resulting in a 7-8 Hz volumetric scanning rate.

4.5 Measurement of fly locomotion and head grooming

The fly stood on a 9-mm track ball made of white foam (FR-4615, General Plastics) painted with irregular black shapes. The ball floated above a 3D-printed plenum (Form 2 printer with Grey Pro resin, Formlabs). Medical-grade breathing air flowed into the base of the plenum and flowed out through a hemispherical depression that cradled the ball. The track ball was illuminated by a round board of 36 infrared LED lamps (SODIAL) positioned behind the fly, as well as an infrared LED flashlight positioned to the left of the fly (850 nm, Amazon).

For experiments in which we monitored locomotion (Figure 2), the ball's movement was captured using a video camera positioned behind the fly (CM3-U3-13Y3M, FLIR) fitted with a 94mm/0.5× Infinistix lens (Infinity Co.). Machine vision software (FicTrac; Moore et al., 2014) converted the image of the ball to an estimate of its position in all three axes of rotation at a rate of 50 Hz. The rotational displacement data was used to calculate the fly's rotational velocity at each time point. The velocity data was smoothed repeatedly 5 times with a Gaussian kernel 5 samples in width prior to data analysis.

For experiments in which we monitored head grooming, video was acquired from a camera focused on the left side of the fly (BFLY-U3-23S6M, FLIR) fitted with a 94mm/1.0× Infinistix lens and 900 nm short-pass filter (Edmund Optics #64335). In imaging experiments, video frames were acquired at 30 Hz. For the experiments in which we tracked the movement of the tibia without imaging (Figure 6), video was acquired at a higher frame rate of 90 Hz.

4.6 Visual stimulus delivery

Visual stimuli were presented using a circular panorama made of modular LED panels (Isaacson *et al.*, 2022). Each LED panel was made up of a 16×16 array of blue LEDs (465 nm peak). The panels were arranged to create a semi-cylindrical arena spanning 300° of visual space along the azimuth and 45° vertically. The space behind the fly was devoid of LED panels in order to accommodate the infrared light source and camera for locomotion tracking. With the fly mounted at the center of the visual panorama, individual LED “pixels” subtended approximately 1.9° of visual space. The visual display was mounted on a vertical manipulator that allowed us to raise and lower the arena to present visual stimuli to the fly (VAP4, Thorlabs). The LED panels were covered with one layer of diffuser film (SXF-0600 Snow White, Decorative Films) to minimize reflections, plus five layers of blue filter gel (Deeper Blue #085, Rosco) to prevent light from the visual display from contaminating the GCaMP emission signals detected by the PMT. The display system was controlled at a refresh rate of 500 Hz using software tools provided by Michael Reiser (<https://reiserlab.github.io/Modular-LED-Display/G4/>). The panorama controller was connected to a breakout box (CB-68LPR, National Instruments) to output the visual stimulus as a voltage signal which was digitized at 10 kHz.

We presented visual stimuli to both control flies and blind flies to verify that LT52 neurons did not respond to visual stimuli in blind flies (data not shown). Before presenting visual stimuli we removed the fly's ipsilateral front leg (that is, on the same side that we were imaging from) to prevent spontaneous leg movements from interfering with our measurements of visual tuning. Visual stimuli were presented for 1s and separated by a 3s interstimulus interval, with a minimum of 15 repetitions of each stimulus. During the interstimulus period, the screen was uniformly illuminated at 50% intensity. The stimulus values shown in Figure 7 are rounded to the nearest 10°/s (motion speed) or nearest ° (grating width).

4.7 Data analysis

Calcium imaging alignment and data processing

All data analysis was performed using Matlab 2022a (Mathworks). Rigid motion correction in the x and y axes was performed for each acquisition using the NoRMCorre algorithm (Pnevmatikakis and Giovannucci, 2017). To verify that fluorescence changes during head grooming were not due to motion artifacts, we manually inspected the quality of the registration for each imaging trial and also confirmed that non-neuronal landmarks within the imaging volume did not show grooming-related signal fluctuations. Volumetric regions of interest (ROIs) were defined by combining 2D ROIs drawn in multiple imaging planes. Fluorescence values were determined by averaging all pixels within that volumetric ROI. $\Delta F/F$ was calculated by finding the 5th percentile of fluorescence values for an ROI within each imaging trial, defining this as the baseline fluorescence value (F), and then computing the change in fluorescence from baseline, divided by this baseline value.

Responses to visual stimuli were computed by averaging the response over 15 or more stimulus repetitions. Stimulus timing and identity were extracted from the voltage output of the LED panels. Prior to averaging, the responses to individual stimulus repetitions were aligned by baseline subtracting the median fluorescence in the 1 s before stimulus onset. The $\Delta F/F$ values plotted in Figure 7 correspond to the peak of the repetition-averaged response within the first 2 s after stimulus onset.

Leg tracking

To track leg movements, we used the machine learning software Animal Part Tracker (<https://kristinbranson.github.io/APT/>) with a Mixture Density Model (MDN) deep convolutional network.

For tracking leg movements during imaging (Figures 3, 4 and 5), the classifier was trained to predict the location of the distal tips of the left and right forelegs and the most ventral point on the left eye. In the text, we refer to the z position of this fixed point as “eye level.” The leg position traces were filtered to remove occasional outlier values that exceeded eye level for only a single frame. These values were replaced with the median of the values before and after it. In Figure 4e, the time of leg elevation was defined as the moment when the ipsilateral leg transitioned from being below eye level (for 0.5 seconds or longer) to being above eye level (for 0.5 seconds or longer).

For the fine-scale analysis of leg movements (Figure 6), the classifier was trained to predict the location of each joint on the left leg, the midpoint of the left tibia, and three fixed points on the left eye. These three fixed points corresponded to the most ventral, most anterior, and most posterior points on the eye that were visible below the surface of the fly holder. The x

and z position traces for each moving point were smoothed with a Gaussian kernel 5 samples wide. The position of the tibia midpoint was converted from units of millimeters to degrees based on the distance between the most posterior and anterior points on the eye, which spans approximately 180° of visual space on the horizontal axis (Heisenberg and Wolf, 1984). The same conversion factor was used for both the x and z axes. Spectral analysis of tibia movement was performed on individual grooming bouts in which the tibia remained above eye level for 1s or longer. For each such bout, the tibia movement traces in x and z were mean-subtracted and analyzed with Matlab's `pspectrum` function. The width of tibia in degrees was estimated based on the diameter and viewing angle of individual ommatidia in the compound eye and the measured width of the tibia at its widest point (Gonzalez-Bellido, Wardill and Juusola, 2011; Posnien *et al.*, 2012).

Connectomics

Connectomics data were obtained from the FlyWire dataset at flywire.ai and the hemibrain dataset at neuprint.janelia.org (Zheng *et al.*, 2018; Scheffer *et al.*, 2020; Dorkenwald *et al.*, 2023) and visualized using the neuPrint and Codex browser query tools.

5. Bibliography

Aimon, S. *et al.* (2023) ‘Global change in brain state during spontaneous and forced walk in *Drosophila* is composed of combined activity patterns of different neuron classes’, *eLife*, 12. Available at: <https://doi.org/10.7554/eLife.85202>.

Åström, K.J. and Murray, R.M. (2010) *Feedback Systems: An Introduction for Scientists and Engineers*. Princeton University Press.

Bell, C. *et al.* (1995) ‘Electric organ corollary discharge pathways in mormyrid fish’, *Journal of Comparative Physiology A*, 177(4), pp. 449–462. Available at: <https://doi.org/10.1007/BF00187481>.

Bell, C.C. (1981) ‘An efference copy which is modified by reafferent input’, *Science*, 214(4519), pp. 450–453. Available at: <https://doi.org/10.1126/science.7291985>.

Bell, C.C. *et al.* (1993) ‘Storage of a sensory pattern by anti-Hebbian synaptic plasticity in an electric fish’, *Proceedings of the National Academy of Sciences of the United States of America*, 90(10), pp. 4650–4654. Available at: <https://doi.org/10.1073/pnas.90.10.4650>.

Bell, C.C. *et al.* (1997) ‘Synaptic plasticity in a cerebellum-like structure depends on temporal order’, *Nature*, 387(6630), pp. 278–281. Available at: <https://doi.org/10.1038/387278a0>.

Bell, C.C. and Grant, K. (1989) ‘Corollary discharge inhibition and preservation of temporal information in a sensory nucleus of mormyrid electric fish’, *The Journal of neuroscience: the official journal of the Society for Neuroscience*, 9(3), pp. 1029–1044. Available at: <https://doi.org/10.1523/JNEUROSCI.09-03-01029.1989>.

Bell, C.C., Libouban, S. and Szabo, T. (1983) ‘Pathways of the electric organ discharge command and its corollary discharges in mormyrid fish’, *The Journal of comparative neurology*, 216(3), pp. 327–338. Available at: <https://doi.org/10.1002/cne.902160309>.

Bell, C. and von der Emde, G. (1995) ‘Electric organ corollary discharge pathways in mormyrid fish’, *Journal of Comparative Physiology A*, 177(4), pp. 463–479. Available at: <https://doi.org/10.1007/BF00187482>.

Binda, P. and Morrone, M.C. (2018) ‘Vision During Saccadic Eye Movements’, *Annual review of vision science*, 4, pp. 193–213. Available at: <https://doi.org/10.1146/annurev-vision-091517-034317>.

Blakemore, S.J., Frith, C.D. and Wolpert, D.M. (1999) ‘Spatio-temporal prediction modulates the perception of self-produced stimuli’, *Journal of cognitive neuroscience*, 11(5), pp. 551–559. Available at: <https://doi.org/10.1162/089892999563607>.

Brezovec, B.E. *et al.* (2024) ‘Mapping the neural dynamics of locomotion across the *Drosophila* brain’, *Current biology: CB*, 34(4), pp. 710–726.e4. Available at: <https://doi.org/10.1016/j.cub.2023.12.063>.

Brooks, J.X., Carriot, J. and Cullen, K.E. (2015) ‘Learning to expect the unexpected: rapid updating in primate cerebellum during voluntary self-motion’, *Nature neuroscience*, 18(9), pp. 1310–1317. Available at: <https://doi.org/10.1038/nn.4077>.

Brooks, J.X. and Cullen, K.E. (2009) ‘Multimodal integration in rostral fastigial nucleus provides an estimate of body movement’, *The Journal of neuroscience: the official journal of the Society for*

Neuroscience, 29(34), pp. 10499–10511. Available at:
<https://doi.org/10.1523/JNEUROSCI.1937-09.2009>.

Brooks, J.X. and Cullen, K.E. (2013) ‘The primate cerebellum selectively encodes unexpected self-motion’, *Current biology: CB*, 23(11), pp. 947–955. Available at:
<https://doi.org/10.1016/j.cub.2013.04.029>.

Bryan, J.S. and Krasne, F.B. (1977) ‘Protection from habituation of the crayfish lateral giant fibre escape response’, *The Journal of physiology*, 271(2), pp. 351–368. Available at:
<https://doi.org/10.1113/jphysiol.1977.sp012004>.

Chen, S. *et al.* (2002) ‘Fighting fruit flies: a model system for the study of aggression’, *Proceedings of the National Academy of Sciences of the United States of America*, 99(8), pp. 5664–5668. Available at:
<https://doi.org/10.1073/pnas.082102599>.

Crapse, T.B. and Sommer, M.A. (2008) ‘Corollary discharge across the animal kingdom’, *Nature reviews. Neuroscience*, 9(8), pp. 587–600. Available at: <https://doi.org/10.1038/nrn2457>.

Cruz, T.L., Pérez, S.M. and Chiappe, M.E. (2021) ‘Fast tuning of posture control by visual feedback underlies gaze stabilization in walking *Drosophila*’, *Current biology: CB*, 31(20), pp. 4596–4607.e5. Available at: <https://doi.org/10.1016/j.cub.2021.08.041>.

Cullen, K.E. (2004) ‘Sensory signals during active versus passive movement’, *Current opinion in neurobiology*, 14(6), pp. 698–706. Available at: <https://doi.org/10.1016/j.conb.2004.10.002>.

Cullen, K.E. *et al.* (2011) ‘Internal models of self-motion: computations that suppress vestibular reafference in early vestibular processing’, *Experimental brain research. Experimentelle Hirnforschung. Experimentation cerebrale*, 210(3-4), pp. 377–388. Available at:
<https://doi.org/10.1007/s00221-011-2555-9>.

Davis, W.J., Siegler, M.V. and Mpitoses (1973) ‘Distributed neuronal oscillators and efference copy in the feeding system of *Pleurobranchaea*’, *Journal of neurophysiology*, 36(2), pp. 258–274. Available at:
<https://doi.org/10.1152/jn.1973.36.2.258>.

Dickinson, M.H. and Muijres, F.T. (2016) ‘The aerodynamics and control of free flight manoeuvres in *Drosophila*’, *Philosophical transactions of the Royal Society of London. Series B, Biological sciences*, 371(1704). Available at: <https://doi.org/10.1098/rstb.2015.0388>.

Dorkenwald, S. *et al.* (2023) ‘Neuronal wiring diagram of an adult brain’, *bioRxiv : the preprint server for biology* [Preprint]. Available at: <https://doi.org/10.1101/2023.06.27.546656>.

Duhamel, J.R., Colby, C.L. and Goldberg, M.E. (1992) ‘The updating of the representation of visual space in parietal cortex by intended eye movements’, *Science*, 255(5040), pp. 90–92. Available at:
<https://doi.org/10.1126/science.1553535>.

Eichler, K. *et al.* (2023) ‘Somatotopic organization among parallel sensory pathways that promote a grooming sequence in *Drosophila*’, *bioRxiv : the preprint server for biology* [Preprint]. Available at:
<https://doi.org/10.1101/2023.02.11.528119>.

Fenk, L.M., Kim, A.J. and Maimon, G. (2021) ‘Suppression of motion vision during course-changing, but not course-stabilizing, navigational turns’, *Current biology: CB*, 31(20), pp. 4608–4619.e3. Available at:
<https://doi.org/10.1016/j.cub.2021.09.068>.

- Fernandez, M.P., Trannoy, S. and Certel, S.J. (2023) ‘Fighting Flies: Quantifying and Analyzing *Drosophila* Aggression’, *Cold Spring Harbor protocols*, 2023(9), p. db.top107985. Available at: <https://doi.org/10.1101/pdb.top107985>.
- Frith, C.D. (1992) ‘The cognitive neuropsychology of schizophrenia’, *Essays in cognitive psychology*, 169. Available at: <https://psycnet.apa.org/fulltext/1993-97187-000.pdf>.
- Fujiwara, T. *et al.* (2017) ‘A faithful internal representation of walking movements in the *Drosophila* visual system’, *Nature neuroscience*, 20(1), pp. 72–81. Available at: <https://doi.org/10.1038/nn.4435>.
- Fujiwara, T., Brotas, M. and Chiappe, M.E. (2022) ‘Walking strides direct rapid and flexible recruitment of visual circuits for course control in *Drosophila*’, *Neuron*, 110(13), pp. 2124–2138.e8. Available at: <https://doi.org/10.1016/j.neuron.2022.04.008>.
- Fukutomi, M. and Carlson, B.A. (2020) ‘A History of Corollary Discharge: Contributions of Mormyrid Weakly Electric Fish’, *Frontiers in integrative neuroscience*, 14, p. 42. Available at: <https://doi.org/10.3389/fnint.2020.00042>.
- Gallagher, I., I. (2000) ‘Philosophical conceptions of the self: implications for cognitive science’, *Trends in cognitive sciences*, 4(1), pp. 14–21. Available at: [https://doi.org/10.1016/s1364-6613\(99\)01417-5](https://doi.org/10.1016/s1364-6613(99)01417-5).
- Gonzalez-Bellido, P.T., Wardill, T.J. and Juusola, M. (2011) ‘Compound eyes and retinal information processing in miniature dipteran species match their specific ecological demands’, *Proceedings of the National Academy of Sciences of the United States of America*, 108(10), pp. 4224–4229. Available at: <https://doi.org/10.1073/pnas.1014438108>.
- Hampel, S. *et al.* (2015) ‘A neural command circuit for grooming movement control’, *eLife*, 4, p. e08758. Available at: <https://doi.org/10.7554/eLife.08758>.
- Hampel, S. *et al.* (2017) ‘Simultaneous activation of parallel sensory pathways promotes a grooming sequence in *Drosophila*’, *eLife*, 6. Available at: <https://doi.org/10.7554/eLife.28804>.
- Heiligenberg, W. (1969) ‘The effect of stimulus chirps on a cricket’s chirping (*Acheta domesticus*)’, *Zeitschrift für vergleichende Physiologie*, 65(1), pp. 70–97. Available at: <https://doi.org/10.1007/BF00297990>.
- Heisenberg, M. and Wolf, R. (1984) *Vision in Drosophila*. Springer Berlin Heidelberg. Available at: <https://doi.org/10.1007/978-3-642-69936-8>.
- von Helmholtz, H. (1867) *Handbuch der physiologischen Optik*. Leipzig: Leopold Voss.
- Hindmarsh Sten, T. *et al.* (2021) ‘Sexual arousal gates visual processing during *Drosophila* courtship’, *Nature*, 595(7868), pp. 549–553. Available at: <https://doi.org/10.1038/s41586-021-03714-w>.
- von Holst, E. and Mittelstaedt, H. (1950) ‘Das Reafferenzprinzip’, *Die Naturwissenschaften*, 37(20), pp. 464–476. Available at: <https://doi.org/10.1007/BF00622503>.
- Isaacson, M. *et al.* (2022) ‘A high-speed, modular display system for diverse neuroscience applications’, *bioRxiv*. Available at: <https://doi.org/10.1101/2022.08.02.502550>.
- Johansson, R.S. and Cole, K.J. (1992) ‘Sensory-motor coordination during grasping and manipulative actions’, *Current opinion in neurobiology*, 2(6), pp. 815–823. Available at: [https://doi.org/10.1016/0959-4388\(92\)90139-c](https://doi.org/10.1016/0959-4388(92)90139-c).

- Keleş, M.F. and Frye, M.A. (2017) ‘Object-Detecting Neurons in *Drosophila*’, *Current biology: CB*, 27(5), pp. 680–687. Available at: <https://doi.org/10.1016/j.cub.2017.01.012>.
- Kim, A.J. *et al.* (2017) ‘Quantitative Predictions Orchestrate Visual Signaling in *Drosophila*’, *Cell*, 168(1-2), pp. 280–294.e12. Available at: <https://doi.org/10.1016/j.cell.2016.12.005>.
- Kim, A.J., Fitzgerald, J.K. and Maimon, G. (2015) ‘Cellular evidence for efference copy in *Drosophila* visuomotor processing’, *Nature neuroscience*, 18(9), pp. 1247–1255. Available at: <https://doi.org/10.1038/nn.4083>.
- Klapoetke, N.C. *et al.* (2022) ‘A functionally ordered visual feature map in the *Drosophila* brain’, *Neuron*, 110(10), pp. 1700–1711.e6. Available at: <https://doi.org/10.1016/j.neuron.2022.02.013>.
- Kovac, M.P. and Davis, W.J. (1980) ‘Neural mechanism underlying behavioral choice in *Pleurobranchaea*’, *Journal of neurophysiology*, 43(2), pp. 469–487. Available at: <https://doi.org/10.1152/jn.1980.43.2.469>.
- Krasne, F.B. and Bryan, J.S. (1973) ‘Habituation: regulation through presynaptic inhibition’, *Science*, 182(4112), pp. 590–592. Available at: <https://doi.org/10.1126/science.182.4112.590>.
- Laurens, J. and Angelaki, D.E. (2017) ‘A unified internal model theory to resolve the paradox of active versus passive self-motion sensation’, *eLife*, 6. Available at: <https://doi.org/10.7554/eLife.28074>.
- Luan, H. *et al.* (2006) ‘Refined spatial manipulation of neuronal function by combinatorial restriction of transgene expression’, *Neuron*, 52(3), pp. 425–436. Available at: <https://doi.org/10.1016/j.neuron.2006.08.028>.
- Markram, H., Gerstner, W. and Sjöström, P.J. (2011) ‘A history of spike-timing-dependent plasticity’, *Frontiers in synaptic neuroscience*, 3, p. 4. Available at: <https://doi.org/10.3389/fnsyn.2011.00004>.
- McKay, R.R. *et al.* (1995) ‘Phospholipase C Rescues Visual Defect in *norpA* Mutant of *Drosophila melanogaster*’, *The Journal of biological chemistry*, 270(22), pp. 13271–13276. Available at: <https://doi.org/10.1074/jbc.270.22.13271>.
- Miller, A. and Demerec, M. (1950) ‘Biology of *Drosophila*’, *The internal anatomy and histology of the imago of *Drosophila melanogaster** [Preprint].
- Mohr, C., Roberts, P.D. and Bell, C.C. (2003a) ‘The mormyromast region of the mormyrid electrosensory lobe. II. Responses to input from central sources’, *Journal of neurophysiology*, 90(2), pp. 1211–1223. Available at: <https://doi.org/10.1152/jn.00213.2003>.
- Mohr, C., Roberts, P.D. and Bell, C.C. (2003b) ‘The mormyromast region of the mormyrid electrosensory lobe. I. Responses to corollary discharge and electrosensory stimuli’, *Journal of neurophysiology*, 90(2), pp. 1193–1210. Available at: <https://doi.org/10.1152/jn.00211.2003>.
- Morimoto, M.M. *et al.* (2020) ‘Spatial readout of visual looming in the central brain of *Drosophila*’, *eLife*, 9. Available at: <https://doi.org/10.7554/eLife.57685>.
- Otsuna, H. and Ito, K. (2006) ‘Systematic analysis of the visual projection neurons of *Drosophila melanogaster*. I. Lobula-specific pathways’, *The Journal of comparative neurology*, 497(6), pp. 928–958. Available at: <https://doi.org/10.1002/cne.21015>.
- Pak, W.L., Grossfield, J. and Arnold, K.S. (1970) ‘Mutants of the visual pathway of *Drosophila*

- melanogaster', *Nature*, 227(5257), pp. 518–520. Available at: <https://doi.org/10.1038/227518b0>.
- Panser, K. *et al.* (2016) 'Automatic Segmentation of Drosophila Neural Compartments Using GAL4 Expression Data Reveals Novel Visual Pathways', *Current biology: CB*, 26(15), pp. 1943–1954. Available at: <https://doi.org/10.1016/j.cub.2016.05.052>.
- Pfeiffer, B.D. *et al.* (2010) 'Refinement of tools for targeted gene expression in Drosophila', *Genetics*, 186(2), pp. 735–755. Available at: <https://doi.org/10.1534/genetics.110.119917>.
- Pick, S. and Strauss, R. (2005) 'Goal-driven behavioral adaptations in gap-climbing Drosophila', *Current biology: CB*, 15(16), pp. 1473–1478. Available at: <https://doi.org/10.1016/j.cub.2005.07.022>.
- Pnevmatikakis, E.A. and Giovannucci, A. (2017) 'NoRMCorre: An online algorithm for piecewise rigid motion correction of calcium imaging data', *Journal of neuroscience methods*, 291, pp. 83–94. Available at: <https://doi.org/10.1016/j.jneumeth.2017.07.031>.
- Posnien, N. *et al.* (2012) 'Evolution of eye morphology and rhodopsin expression in the Drosophila melanogaster species subgroup', *PloS one*, 7(5), p. e37346. Available at: <https://doi.org/10.1371/journal.pone.0037346>.
- Poulet, J.F.A. and Hedwig, B. (2002) 'A corollary discharge maintains auditory sensitivity during sound production', *Nature*, 418(6900), pp. 872–876. Available at: <https://doi.org/10.1038/nature00919>.
- Poulet, J.F.A. and Hedwig, B. (2003) 'A corollary discharge mechanism modulates central auditory processing in singing crickets', *Journal of neurophysiology*, 89(3), pp. 1528–1540. Available at: <https://doi.org/10.1152/jn.0846.2002>.
- Poulet, J.F.A. and Hedwig, B. (2003) 'Corollary discharge inhibition of ascending auditory neurons in the stridulating cricket', *The Journal of neuroscience: the official journal of the Society for Neuroscience*, 23(11), pp. 4717–4725. Available at: <https://doi.org/10.1523/JNEUROSCI.23-11-04717.2003>.
- Poulet, J.F.A. and Hedwig, B. (2006) 'The cellular basis of a corollary discharge', *Science*, 311(5760), pp. 518–522. Available at: <https://doi.org/10.1126/science.1120847>.
- Poulet, J.F.A. and Hedwig, B. (2007) 'New insights into corollary discharges mediated by identified neural pathways', *Trends in neurosciences*, 30(1), pp. 14–21. Available at: <https://doi.org/10.1016/j.tins.2006.11.005>.
- Qiao, B. *et al.* (2018) 'Automated analysis of long-term grooming behavior in Drosophila using a k-nearest neighbors classifier', *eLife*, 7. Available at: <https://doi.org/10.7554/eLife.34497>.
- Requarth, T., Kaifosh, P. and Sawtell, N.B. (2014) 'A role for mixed corollary discharge and proprioceptive signals in predicting the sensory consequences of movements', *The Journal of neuroscience: the official journal of the Society for Neuroscience*, 34(48), pp. 16103–16116. Available at: <https://doi.org/10.1523/JNEUROSCI.2751-14.2014>.
- Ribeiro, I.M.A. *et al.* (2018) 'Visual Projection Neurons Mediating Directed Courtship in Drosophila', *Cell*, 174(3), pp. 607–621.e18. Available at: <https://doi.org/10.1016/j.cell.2018.06.020>.
- Roy, J.E. and Cullen, K.E. (2004) 'Dissociating self-generated from passively applied head motion: neural mechanisms in the vestibular nuclei', *The Journal of neuroscience: the official journal of the Society for Neuroscience*, 24(9), pp. 2102–2111. Available at: <https://doi.org/10.1523/JNEUROSCI.3988-03.2004>.

- Schaffer, E.S. *et al.* (2023) ‘The spatial and temporal structure of neural activity across the fly brain’, *Nature communications*, 14(1), p. 5572. Available at: <https://doi.org/10.1038/s41467-023-41261-2>.
- Scheffer, L.K. *et al.* (2020) ‘A connectome and analysis of the adult *Drosophila* central brain’, *eLife*, 9. Available at: <https://doi.org/10.7554/eLife.57443>.
- Schretter, C.E. *et al.* (2020) ‘Cell types and neuronal circuitry underlying female aggression in *Drosophila*’, *eLife*, 9. Available at: <https://doi.org/10.7554/eLife.58942>.
- Schretter, C.E. *et al.* (2024) ‘Social state gates vision using three circuit mechanisms in *Drosophila*’, *bioRxiv*. Available at: <https://doi.org/10.1101/2024.03.15.585289>.
- Singla, S. *et al.* (2017) ‘A cerebellum-like circuit in the auditory system cancels responses to self-generated sounds’, *Nature neuroscience*, 20(7), pp. 943–950. Available at: <https://doi.org/10.1038/nn.4567>.
- Sirigu, A. *et al.* (1999) ‘Perception of self-generated movement following left parietal lesion’, *Brain: a journal of neurology*, 122 (Pt 10), pp. 1867–1874. Available at: <https://doi.org/10.1093/brain/122.10.1867>.
- Sommer, M.A. and Wurtz, R.H. (2002) ‘A pathway in primate brain for internal monitoring of movements’, *Science*, 296(5572), pp. 1480–1482. Available at: <https://doi.org/10.1126/science.1069590>.
- Sommer, M.A. and Wurtz, R.H. (2004) ‘What the brain stem tells the frontal cortex. II. Role of the SC-MD-FEF pathway in corollary discharge’, *Journal of neurophysiology*, 91(3), pp. 1403–1423. Available at: <https://doi.org/10.1152/jn.00740.2003>.
- Sommer, M.A. and Wurtz, R.H. (2006) ‘Influence of the thalamus on spatial visual processing in frontal cortex’, *Nature*, 444(7117), pp. 374–377. Available at: <https://doi.org/10.1038/nature05279>.
- Sperry, R.W. (1950) ‘Neural basis of the spontaneous optokinetic response produced by visual inversion’, *Journal of comparative and physiological psychology*, 43(6), pp. 482–489. Available at: <https://doi.org/10.1037/h0055479>.
- Srinivasan, M.V., Laughlin, S.B. and Dubs, A. (1982) ‘Predictive coding: a fresh view of inhibition in the retina’, *Proceedings of the Royal Society of London. Series B, Containing papers of a Biological character. Royal Society*, 216(1205), pp. 427–459. Available at: <https://doi.org/10.1098/rspb.1982.0085>.
- Straka, H., Simmers, J. and Chagnaud, B.P. (2018) ‘A New Perspective on Predictive Motor Signaling’, *Current biology: CB*, 28(5), pp. R232–R243. Available at: <https://doi.org/10.1016/j.cub.2018.01.033>.
- Strother, J.A. *et al.* (2018) ‘Behavioral state modulates the ON visual motion pathway of *Drosophila*’, *Proceedings of the National Academy of Sciences of the United States of America*, 115(1), pp. E102–E111. Available at: <https://doi.org/10.1073/pnas.1703090115>.
- Turner, M.H. *et al.* (2022) ‘Visual and motor signatures of locomotion dynamically shape a population code for feature detection in *Drosophila*’, *eLife*, 11. Available at: <https://doi.org/10.7554/eLife.82587>.
- Tuthill, J.C. and Wilson, R.I. (2016) ‘Mechanosensation and Adaptive Motor Control in Insects’, *Current biology: CB*, 26(20), pp. R1022–R1038. Available at: <https://doi.org/10.1016/j.cub.2016.06.070>.
- Umeno, M.M. and Goldberg, M.E. (1997) ‘Spatial processing in the monkey frontal eye field. I. Predictive visual responses’, *Journal of neurophysiology*, 78(3), pp. 1373–1383. Available at:

<https://doi.org/10.1152/jn.1997.78.3.1373>.

Wolpert, D.M. and Ghahramani, Z. (2000) 'Computational principles of movement neuroscience', *Nature neuroscience*, 3 Suppl, pp. 1212–1217. Available at: <https://doi.org/10.1038/81497>.

Wu, M. *et al.* (2016) 'Visual projection neurons in the *Drosophila* lobula link feature detection to distinct behavioral programs', *eLife*, 5. Available at: <https://doi.org/10.7554/eLife.21022>.

Wurtz, R.H. (2018) 'Corollary Discharge Contributions to Perceptual Continuity Across Saccades', *Annual review of vision science*, 4, pp. 215–237. Available at: <https://doi.org/10.1146/annurev-vision-102016-061207>.

Zheng, Z. *et al.* (2018) 'A Complete Electron Microscopy Volume of the Brain of Adult *Drosophila melanogaster*', *Cell*, 174(3), pp. 730–743.e22. Available at: <https://doi.org/10.1016/j.cell.2018.06.019>.

Zipser, B. and Bennett, M.V. (1976) 'Interaction of electrosensory and electromotor signals in lateral line lobe of a mormyrid fish', *Journal of neurophysiology*, 39(4), pp. 713–721. Available at: <https://doi.org/10.1152/jn.1976.39.4.713>.

Zwarts, L., Versteven, M. and Callaerts, P. (2012) 'Genetics and neurobiology of aggression in *Drosophila*', *Fly*, 6(1), pp. 35–48. Available at: <https://doi.org/10.4161/fly.19249>.